




Switch and phase shift of photon polarization qubits via double Rydberg electromagnetically induced transparency

Yao Ou ¹ and Guoxiang Huang ^{1,2,3,*}

¹State Key Laboratory of Precision Spectroscopy, East China Normal University, Shanghai 200241, China

²NYU-ECNU Joint Institute of Physics, New York University Shanghai, Shanghai 200062, China

³Collaborative Innovation Center of Extreme Optics, Shanxi University, Taiyuan 030006, China

 (Received 22 August 2023; revised 31 October 2023; accepted 11 January 2024; published 7 February 2024)

We propose and analyze a scheme for manipulating the propagation of single-photon pulses with two polarization components in a Rydberg atomic gas via double electromagnetically induced transparency. We show that by storing a gate photon in a Rydberg state, a deep and tunable potential for a photon polarization qubit can be achieved based on the strong Rydberg interaction. We also show that the scheme can be used to realize an all-optical switch in the dissipation regime and generate a large phase shift in the dispersion regime for the photon polarization qubit. Moreover, we demonstrate that such a scheme can be utilized to detect weak magnetic fields. The results reported here are not only beneficial for understanding the quantum optical property of Rydberg atomic gases, but also promising for designing devices for quantum information processing.

DOI: [10.1103/PhysRevA.109.023508](https://doi.org/10.1103/PhysRevA.109.023508)

I. INTRODUCTION

Photons do not interact with each other in vacuum and also hardly interact with their environments. The linear (or nearly linear) property of light propagation, in combination with high speed, large bandwidth, and low loss, has made photons excellent information carriers for optical communications over long distances. However, for quantum information processing, strong interactions between photons are required. Although interactions between photons may be obtained through some nonlinear optical processes [1], optical nonlinearities realized through these processes are too weak for all-optical quantum information processing.

An all-optical switch is a photonic device by which a gate pulse can effectively change the transmission of a target pulse without the aid of electronic techniques. For quantum information processing, it is desirable to build single-photon switches in which the gate pulse contains only one photon. However, building single-photon switches is generally difficult, because Kerr nonlinearities in conventional optical media are too small at single-photon levels. Nevertheless, the research of electromagnetically induced transparency (EIT) [2] in the past three decades has led to the possibility of realizing strong optical nonlinearities at few-photon levels [3].

Among a wide variety of physical systems that support EITs, Rydberg atomic gases [4,5] are particularly attractive, in which the strong atom-atom interaction can be effectively mapped onto the strong photon-photon interaction via Rydberg EIT [6–8]. In recent years, tremendous attention has been paid to the study of various single- and few-photon states and their quantum dynamics in atomic gases working under the condition of Rydberg EIT [9–32]. In particular, many

single-photon devices (including single-photon switches and phase gates), which are promising for all-optical quantum information processing, have been demonstrated experimentally [31–46].

In this article we suggest a scheme to realize a single-photon switch based on the strong Rydberg interaction. Different from those schemes explored before, in which single-photon switches were designed for photon states with only one polarization component $|\sigma\rangle$ [15,17,19,35–38], in our scheme the single-photon switch is for the photon state with two polarization components σ^+ and σ^- , i.e., for photon polarization qubit $c_+|\sigma^+\rangle + c_-|\sigma^-\rangle$ (c_+ and c_- are complex constants satisfying $|c_+|^2 + |c_-|^2 = 1$). The system we consider is a cold Rydberg atomic gas working under the condition of double Rydberg EIT. Recently, such EIT has been used to acquire large self- and cross-Kerr nonlinearities and some nonlinear optical phenomena (e.g., giant magneto-optical rotation, self-organized optical spatial structures, and Stern-Gerlach deflection of light bullets) for situations with large probe photon numbers [47–51]. In contrast with these works, where semiclassical approaches were used, in the present study the probe-laser field in the system is assumed to be in a single-photon state; hence an all-quantum approach for both the atoms and the probe field is needed.

We show that, by storing a gate photon in a Rydberg state, a deep and tunable optical potential (called Rydberg-defect potential below) for a photon polarization qubit can be prepared through the strong Rydberg interaction. We also show that by using this scheme it is possible to design an effective switch for the photon polarization qubit if the system works in the dissipation regime. Moreover, large phase shifts for the two polarization components of the photon polarization qubit can be generated when the system works in the dispersion regime. In addition, we demonstrate that such a scheme can be utilized to detect weak magnetic fields. The research

*gxhuang@phy.ecnu.edu.cn

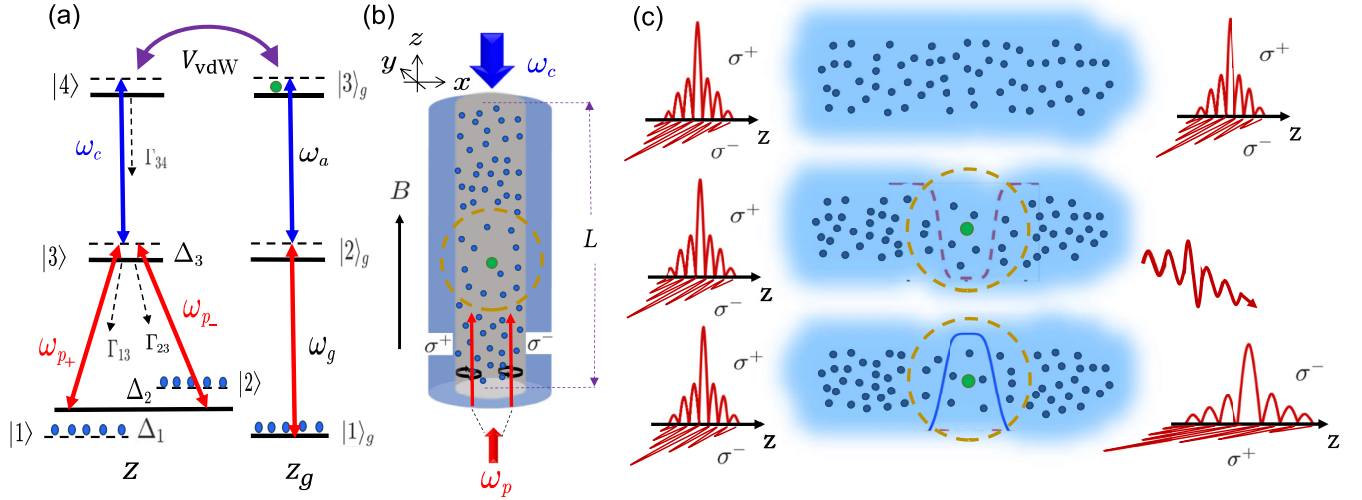


FIG. 1. Schematics of the model and the propagation of the single-photon polarization qubit. (a) Shown on the left is the level diagram and excitation scheme of the double Rydberg EIT, consisting of two ladder-shaped EIT excitation paths, i.e., $|1\rangle \leftrightarrow |3\rangle \leftrightarrow |4\rangle$ and $|2\rangle \leftrightarrow |3\rangle \leftrightarrow |4\rangle$, with $|1\rangle$ and $|2\rangle$ the two lower states, $|3\rangle$ the excited state, and $|4\rangle$ the Rydberg state. Shown on the right is a gate photon stored in another Rydberg state $|3\rangle_g$ of the gate atom via another Rydberg EIT through the excitation path $|1\rangle_g \rightarrow |2\rangle_g \rightarrow |3\rangle_g$. Red (blue) lines with double-headed arrows represent the probe (control) fields. The purple line with double arrows and the symbol V_{vdW} represents the van der Waals interaction between the Rydberg atom located at the position z and the Rydberg atom at the position z_g (gate atom). For a detailed description of the probe and control fields, atomic decay rates $\Gamma_{\alpha\beta}$, and detunings Δ_α , see the text. (b) Suggested geometry of the system. The gate atom (assumed to be located at the middle of the atomic gas, i.e., $z_g = L/2$) excited to the Rydberg state $|3\rangle_g$ by the gate photon is denoted by the green closed circle; other atoms are denoted by smaller blue closed circles. The domain centered at the gate atom forms a Rydberg blockade sphere with radius r_b (indicated by the yellow dashed circle), which contributes a Rydberg-defect potential for the incident probe photon qubit. An external magnetic field B applied in the z direction results in the detunings $\Delta_1 = -\Delta_2 = -\mu_B B/3\hbar$. (c) Shown on top is the schematic of the free propagation of the two polarization components σ_+ and σ_- of the photon qubit in the absence of the stored gate photon, i.e., the qubit switch is off. In the middle the stored gate photon induces a dissipation-type Rydberg-defect potential (with a large imaginary part) indicated by the purple dashed curve, blocking the transmission of the photon qubit, i.e., the qubit switch is on. On the bottom the stored gate photon induces a dispersion-type Rydberg-defect potential (with a large real part) indicated by the blue solid curve. Significant phase shifts are generated for the two polarization components of the photon qubit.

results reported here are useful not only for understanding the quantum optical property of Rydberg atomic gases, but also for designing single-photon devices which are promising for optical quantum information processing [52].

The remainder of the article is arranged as follows. In Sec. II we describe the physical model under study and derive two-component envelope equations of the quantized probe field based on Heisenberg-Maxwell (HM) equations. In Sec. III we solve the two-component envelope equations and present analytical and numerical results on the realization of the Rydberg-defect potential, polarization qubit switch, phase shifts of the two qubit components, and magnetic-field-induced switching behavior for the polarization qubit. In Sec. IV we summarize the main results obtained in this work.

II. MODEL AND EQUATIONS OF MOTION

A. Physical model

We start by considering a cold four-level atomic gas (lower states $|1\rangle$ and $|2\rangle$, excited state $|3\rangle$, and Rydberg state $|4\rangle$) with an excitation scheme of an inverted-Y-type configuration, interacting with a weak, pulsed probe laser field (target pulse) of central wave number k_p and angular frequency $\omega_p = k_p c$,

and a strong continuous-wave control laser field of wave number k_c and angular frequency $\omega_c = k_c c$ [see the left part of Fig. 1(a)]. To suppress the first-order Doppler effect, the probe (control) field is assumed to propagate in the z ($-z$) direction.

We assume that the probe field consists of two polarization components, i.e., a right-circular (σ^+) and a left-circular (σ^-) one, coupling to transitions $|1\rangle \leftrightarrow |3\rangle$ and $|2\rangle \leftrightarrow |3\rangle$, respectively; the control field couples to the transition $|3\rangle \leftrightarrow |4\rangle$. Here Γ_{13} , Γ_{23} , and Γ_{34} are spontaneous decay rates from $|3\rangle$ to $|1\rangle$, $|3\rangle$ to $|2\rangle$, and $|4\rangle$ to $|3\rangle$, respectively. In addition, Δ_1 and Δ_2 are Zeeman energy splittings of the atomic ground-state level, induced by an external magnetic field B applied in the z direction [53]; Δ_3 and Δ_4 are one-photon and two-photon detunings, respectively. The excitation scheme shown in the left part of Fig. 1(a) is the basic configuration of double Rydberg EIT; it consists of two ladder-shaped EIT excitation paths, i.e., $|1\rangle \leftrightarrow |3\rangle \leftrightarrow |4\rangle$ and $|2\rangle \leftrightarrow |3\rangle \leftrightarrow |4\rangle$.

For simplicity, we assume that the system behaves as a one-dimensional one, which can be realized by taking a cigar-shaped atomic gas or an atomic gas filled into a waveguide with small transverse sizes, so that the optical fields of the system in transverse directions are tightly confined, and hence the diffraction effect can be safely neglected. Thereby, a $(1+1)$ -dimensional (i.e., time plus the space along the z axis) model is sufficient to describe the dynamics of the system, as

schematically shown in Fig. 1(b).¹ The total electric field in the system reads

$$\hat{\mathbf{E}}(z, t) = \mathbf{E}_c(z, t) + \hat{\mathbf{E}}_p(z, t), \quad (1a)$$

$$\mathbf{E}_c(z, t) = \mathbf{e}_c \mathcal{E}_c e^{i(-k_c z - \omega_c t)} + \text{c.c.}, \quad (1b)$$

$$\hat{\mathbf{E}}_p(z, t) = \hat{\mathbf{E}}_{p+}(z, t) + \hat{\mathbf{E}}_{p-}(z, t), \quad (1c)$$

$$\hat{\mathbf{E}}_{pj}(z, t) = \mathbf{e}_{pj} \mathcal{E}_p \hat{E}_{pj}(z, t) e^{i(k_{p\pm} z - \omega_{p\pm} t)} + \text{H.c.} \quad (1d)$$

Here $j = +, -$; $k_{p\pm} = k_p$; $\omega_{p\pm} = \omega_p$; c.c. (H.c.) represents the complex (Hermitian) conjugate; \mathbf{e}_c and \mathcal{E}_c are the unit polarization vector and amplitude of the control field, respectively; $\mathcal{E}_p \equiv \sqrt{\hbar \omega_p / 2 \varepsilon_0 V}$ is the field amplitude of a single probe photon, with $V = LA_0$ the optical volume of the system (A_0 and L are the cross-section area and longitudinal size of the atomic ensemble, respectively); and $\mathbf{e}_{p+} = (\mathbf{e}_x + i\mathbf{e}_y)/\sqrt{2}$ and $\hat{E}_{p+}(z, t)$ [$\mathbf{e}_{p-} = (\mathbf{e}_x - i\mathbf{e}_y)/\sqrt{2}$ and $\hat{E}_{p-}(z, t)$] are the unit polarization vector and annihilation operator of probe photon, respectively, for the σ^+ (σ^-)-polarized component. The operators $\hat{E}_{p+}(z, t)$ and $\hat{E}_{p-}(z, t)$ obey commutation relations

$$[\hat{E}_{pj}(z, t), \hat{E}_{pj'}(z', t)] = [\hat{E}_{pj}^\dagger(z, t), \hat{E}_{pj'}^\dagger(z', t)] = 0, \quad (2a)$$

$$[\hat{E}_{pj}(z, t), \hat{E}_{pj'}^\dagger(z', t)] = L \delta(z - z') \delta_{jj'}, \quad (2b)$$

with $j, j' = +, -$ and L the size of the system in the z direction. We also assume that the incident probe field is a single-photon pulse and the quantum state of the pulse is a polarization qubit because the pulse contains two polarization components.

In order to design a switch for the photon polarization qubit, a gate photon must be prepared. Here we adopt the idea used in Refs. [35–38], i.e., before the incidence of the probe photon, a gate photon is stored in another Rydberg state $|3_g\rangle$ of an atom (called the gate atom). This can be realized by using another Rydberg EIT through the excitation path $|1_g\rangle \rightarrow |2_g\rangle \rightarrow |3_g\rangle$. Here the gate photon pulse (with central angular frequency ω_g and half Rabi frequency Ω_g) couples the atomic states $|1_g\rangle$ and $|2_g\rangle$, and a strong, assisted laser field (with central angular frequency ω_a and half Rabi frequency Ω_a) couples the states $|2_g\rangle$ and $|3_g\rangle$, as shown in the right part of Fig. 1(a). In this way, the incident gate photon is stored in the gate atom and hence the Rydberg state $|3\rangle_g$ can have the atomic population of unit probability.

Assume that the atom excited into the state $|4\rangle$ is located at position z . Because both $|3\rangle_g$ and $|4\rangle$ are Rydberg states, there exists a strong Rydberg-Rydberg interaction between the gate atom (at position z_g) and the atom at z . Such an interaction can be described by the van der Waals interaction potential of the form

$$\hbar V_{\text{vdW}}(z_g - z) = -\frac{\hbar C_6}{|z_g - z|^6} \quad (3)$$

if both $|4\rangle$ and $|3_g\rangle$ are taken to be the S state. Here C_6 is called the dispersion coefficient. The Rydberg-Rydberg interaction

results in atomic level shifts and hence induces an important phenomenon, called Rydberg blockade [4,5,31,32], by which only one atom can be excited to Rydberg states in the region of the Rydberg blockade sphere of radius r_b .²

Under electric dipole, rotating-wave, and paraxial approximations, the effective Hamiltonian of the atomic ensemble is given by $\hat{H} = \hat{H}_{\text{AF}} + \hat{H}_{\text{AG}}$, with

$$\begin{aligned} \hat{H}_{\text{AF}} = & -\hbar \int_{-\infty}^{+\infty} dz \rho_a(z) \left(\sum_{\alpha=1}^4 \Delta_\alpha \hat{S}_{\alpha\alpha}(z, t) \right. \\ & + \Omega_c \hat{S}_{34}(z, t) + g_{p+} \hat{S}_{13}(z, t) \hat{E}_{p+}(z, t) \\ & \left. + g_{p-} \hat{S}_{23}(z, t) \hat{E}_{p-}(z, t) + \text{H.c.} \right), \quad (4a) \end{aligned}$$

$$\begin{aligned} \hat{H}_{\text{AG}} = & \int_{-\infty}^{+\infty} dz \rho_a(z) \int_{-\infty}^{+\infty} dz'_g \rho_g(z'_g) \\ & \times [\hat{S}_{33}(z'_g, t) \hbar V_{\text{vdW}}(z'_g - z) \hat{S}_{44}(z, t)], \quad (4b) \end{aligned}$$

where \hat{H}_{AF} is the Hamiltonian describing the atom-light interaction and \hat{H}_{AG} is the one describing the Rydberg-Rydberg interaction between atoms in the Rydberg state $|4\rangle$ and gate atoms in the Rydberg state $|3\rangle_g$. In these expressions, ρ_g is the linear density of gate atoms, ρ_a is the linear density of atoms other than the gate atoms, $\Omega_c = (\mathbf{e}_c \cdot \mathbf{p}_{43}) \mathcal{E}_c / \hbar$ is the half Rabi frequency of the control field, and $g_{p+} \equiv (\mathbf{e}_{p+} \cdot \mathbf{p}_{31}) \mathcal{E}_p / \hbar$ [$g_{p-} \equiv (\mathbf{e}_{p-} \cdot \mathbf{p}_{32}) \mathcal{E}_p / \hbar$] is the single-photon half Rabi frequency denoting the dipole coupling between the σ^+ (σ^-) component of the probe field and the atomic transition $|1\rangle \leftrightarrow |3\rangle$ ($|2\rangle \leftrightarrow |3\rangle$). Here $\mathbf{p}_{\alpha\beta}$ is the electric dipole matrix element associated with the atomic transition from $|\beta\rangle$ to $|\alpha\rangle$ and $g_{p+} \approx g_{p-} = g_p$ due to the symmetry of the level configuration of the double Rydberg EIT. In addition, we have defined $\hat{S}_{\alpha\beta} \equiv |\beta\rangle \langle \alpha| \exp[i(k_\beta - k_\alpha)z - i(\omega_\beta - \omega_\alpha + \Delta_\beta - \Delta_\alpha)t]$ as atomic transition operators related to the states $|\alpha\rangle$ and $|\beta\rangle$ ($\alpha, \beta = 1-4$), with $k_1 = 0$, $k_2 = k_{p+} - k_{p-} = 0$, $k_3 = k_{p+}$, $k_4 = k_{p+} + k_c$, and $\omega_\alpha = E_\alpha / \hbar$ (E_α being the eigenenergy of the atomic state $|\alpha\rangle$) [48]. The $\hat{S}_{\alpha\beta}$ obey the commutation relation

$$\begin{aligned} [\hat{S}_{\alpha\beta}(z, t), \hat{S}_{\mu\nu}(z', t)] = & \frac{L}{N} \delta(z - z') [\delta_{\alpha\nu} \hat{S}_{\mu\beta}(z, t) \\ & - \delta_{\mu\beta} \hat{S}_{\alpha\nu}(z, t)], \end{aligned}$$

with N the total atomic number of the system. Note that, as in Refs. [15,17,35–39,41], when writing (4a) and (4b) we have assumed that ρ_a is small and hence the Rydberg-Rydberg interaction between the atoms excited in the Rydberg state $|4\rangle$ is negligible.

The Zeeman effect induced by the magnetic field B makes the levels $|1\rangle$ and $|2\rangle$ (which are degenerate when $B = 0$) produce splitting $\Delta E = \mu_B g_F^\alpha m_F^\alpha B$. Here μ_B , g_F^α , and m_F^α are the Bohr magneton, gyromagnetic factor, and magnetic quantum number of the atomic state $|\alpha\rangle$, respectively. Therefore, we have $\Delta_2 = -\Delta_1 = (E_2 - E_1)/2\hbar = \mu_{21} B/2\hbar$,

¹The two polarization components have no spatial separation during propagation. The separation plotted in the figure is used to indicate the fact that the photon qubit consists of two polarization components.

²The radius of the Rydberg blockade sphere $r_b \equiv (|C_6| |d_{31}| / |\Omega_c|^2)^{1/6}$ is about 8 μm . To make the (1+1)-dimensional model valid, the condition $\pi r_b^2 > A_0$ must be satisfied.

$\Delta_3 = \omega_p - (E_3 - E_1)/\hbar$, and $\Delta_4 = \omega_p + \omega_c - (E_4 - E_1)/\hbar - \mu_{41}B/\hbar$, with $\mu_{\alpha\beta} = \mu_B(m_F^\alpha g_F^\alpha - m_F^\beta g_F^\beta)$. The derivation of the effective Hamiltonian (4) is similar to that given in Appendix A of Ref. [48].

As indicated above, we are interested in the case of a single gate photon stored in the gate atom located at the position z_g . Thus the gate-atom density is given by $\rho_g(z'_g) = \delta(z'_g - z_g)$, and $\hat{S}_{33}(z_g, t) \approx \hat{I}$ (\hat{I} is the unit matrix). For simplicity, we assume ρ_a is a constant, given by $\rho_a = N/L$. Then the Hamiltonian \hat{H}_{AG} is reduced to the form $\hat{H}_{AG} = \rho_a \int_{-\infty}^{+\infty} dz \hbar \Delta_d(z) \hat{S}_{44}(z, t)$, with

$$\Delta_d(z) = \int_{-\infty}^{+\infty} dz'_g \rho_g(z'_g) \frac{-C_6}{|z'_g - z|^6} = -\frac{C_6}{|z_g - z|^6}. \quad (5)$$

As a result, $\Delta_d(z)$ behaves as a position-dependent detuning, which will contribute an external optical potential, i.e., the Rydberg-defect potential, for the scattering of the incident probe photon polarization qubit (discussed in Sec. III below). The position of the gate atom is assumed to be located at the middle of the atomic gas, i.e., $z_g = L/2$.

The time evolution of the atoms in the system is governed by the Heisenberg equation of motion

$$i \frac{\partial}{\partial t} \hat{S}_{\alpha\beta} = \left[\hat{S}_{\alpha\beta}, \frac{\hat{H}}{\hbar} \right] + i \hat{\mathcal{L}}(\hat{S}_{\alpha\beta}) + i \hat{F}_{\alpha\beta}. \quad (6)$$

Here the term $\hat{\mathcal{L}}(\hat{S}_{\alpha\beta})$ describes the dissipation of $\hat{S}_{\alpha\beta}$ due to spontaneous emission and dephasing and $\hat{F}_{\alpha\beta}$ are δ -correlated Langevin noise operators describing the fluctuations associated with the dissipations $\hat{\mathcal{L}}(\hat{S}_{\alpha\beta})$. Explicit expressions of Eq. (6) are presented in Appendix A. For simplicity, in the present work the dynamics of the gate atom is not considered, which is approximately valid because the lifetime of the Rydberg state is quite long [35–39,41].

The evolution of the probe field is controlled by the Maxwell equation $\partial^2 \hat{\mathbf{E}}_p / \partial z^2 - (1/c^2) \partial^2 \hat{\mathbf{E}}_p / \partial t^2 = (1/\epsilon_0 c^2) \partial^2 \hat{\mathbf{P}}_p / \partial t^2$, with $\hat{\mathbf{P}}_p \equiv \mathcal{N}_a (\mathbf{p}_{31} \hat{S}_{31} + \mathbf{p}_{32} \hat{S}_{32}) e^{i(k_p z - \omega_p t)} + \text{H.c.}$ the polarization intensity, \mathbf{p}_{31} (\mathbf{p}_{32}) the electric dipole matrix element related to the transition from $|3\rangle$ to $|1\rangle$ ($|3\rangle$ to $|2\rangle$), and $\mathcal{N}_a \equiv N/V = \rho_a/A_0$ the volume atomic density. Under the slowly varying approximation, the Maxwell equation is reduced to

$$i \left(\frac{\partial}{\partial z} + \frac{1}{c} \frac{\partial}{\partial t} \right) \hat{E}_{p+} + \frac{g_{p+}^* N}{c} \hat{S}_{31} = 0, \\ i \left(\frac{\partial}{\partial z} + \frac{1}{c} \frac{\partial}{\partial t} \right) \hat{E}_{p-} + \frac{g_{p-}^* N}{c} \hat{S}_{32} = 0. \quad (7)$$

The physical model described above is valid for many alkali-metal atomic gases, such as ^{85}Rb , ^{87}Rb , and ^{88}Sr . In numerical calculations given in the following, we use cold ^{85}Rb gas as an example. The atomic levels for realizing the double Rydberg EIT are selected to be $|1\rangle = |5^2S_{1/2}, F=3, m_F=-1\rangle$, $|2\rangle = |5^2S_{1/2}, F=3, m_F=1\rangle$, $|3\rangle = |5^2P_{3/2}, F=4, m_F=0\rangle$, and $|4\rangle = |6S_{1/2}\rangle$. For $n=n'=68$ (n and n' are principal quantum numbers of the Rydberg states $|4\rangle$ and $|3\rangle_g$, respectively), the van der Waals dispersion parameter reads $C_6 = -2\pi \times 625.6 \text{ GHz } \mu\text{m}^6$, i.e., the Rydberg-

Rydberg interaction is repulsive. Other system parameters are $\Gamma_{12} = \Gamma_{21} = 2\pi \times 0.0016 \text{ MHz}$, $\Gamma_3 = 2\pi \times 6.06 \text{ MHz}$, $\Gamma_4 = 2\pi \times 0.02 \text{ MHz}$, and $\Gamma_{13} = \Gamma_{23} = \Gamma_3/2$.

For the $D2$ line of ^{85}Rb atoms, the gyromagnetic factor of the two lower levels is $g_F = \frac{1}{3}$. Due to the symmetry of the lower-energy-level shifts induced by the magnetic field B , we have

$$\Delta_1 = -\Delta_2 = -\frac{\mu_B B}{3\hbar}. \quad (8)$$

We stress that, due to the choice of magnetic quantum numbers and the linear polarization of the control field, the levels $|3\rangle$ and $|4\rangle$ are not sensitive to the applied magnetic field. Therefore, the dependence on B for Δ_3 and Δ_4 is negligible.

B. Envelope equations of the two-component probe field

To study the propagation of the probe field under the action of the gate photon, we must solve the HM equations (6) and (7). Because the probe field under consideration is at a single-photon level, nonlinear terms in the HM equations are negligible. By employing a Fourier transformation and eliminating atomic variables, we obtain the linear envelope equations describing the dynamics of the two polarization components of the probe field in frequency space

$$\left(i \frac{\partial}{\partial z} + K_j(z, \omega) \right) \tilde{E}_{pj}(z, \omega) = i \tilde{F}_{pj}(z, \omega), \quad (9)$$

where $j = +, -$ and

$$\tilde{E}_{pj}(z, \omega) = \frac{1}{\sqrt{2\pi}} \int_{-\infty}^{\infty} dt \hat{E}_{pj}(z, t) e^{-i\omega t}, \quad (10a)$$

$$K_+(z, \omega) = \frac{\omega}{c} + \frac{|g_p|^2 N}{2c} \frac{[\omega + d_{41} - \Delta_d(z)]}{D_1(\omega)}, \quad (10b)$$

$$K_-(z, \omega) = \frac{\omega}{c} + \frac{|g_p|^2 N}{2c} \frac{[\omega + d_{42} - \Delta_d(z)]}{D_2(\omega)}, \quad (10c)$$

with $D_\alpha(\omega) = |\Omega_c|^2 - (\omega + d_{3\alpha})[\omega + d_{4\alpha} - \Delta_d(z)]$ ($\alpha = 1, 2$). Here $d_{\alpha\beta} = \Delta_\alpha - \Delta_\beta + i\gamma_{\alpha\beta}$ ($\alpha \neq \beta$), $\gamma_{\alpha\beta} \equiv (\Gamma_\alpha + \Gamma_\beta)/2 + \gamma_{\alpha\beta}^{\text{dep}}$, and $\Gamma_\beta \equiv \sum_{\alpha < \beta} \Gamma_{\alpha\beta}$, with $\Gamma_{\alpha\beta}$ the decay rate of the spontaneous emission from the state $|\beta\rangle$ to the state $|\alpha\rangle$ and $\gamma_{\alpha\beta}^{\text{dep}}$ the dephasing rate between $|\alpha\rangle$ and $|\beta\rangle$. The quantities $K_+(z, \omega)$ and $K_-(z, \omega)$ are linear dispersion relations for the σ^+ and σ^- polarization components, respectively. A detailed derivation of Eq. (9) is presented in Appendix B, with explicit expressions of Langevin noise terms $\tilde{F}_{pj}(z, \omega)$ given by Eqs. (B6a) and (B6b).

Note that when deriving Eq. (9) we have, for simplicity, assumed that $\Delta_d(z)$ is a slowly varying function of z . This allows $\Delta_d(z)$ to be approximated as a constant during the Fourier transformation.³ Under the double EIT condition,

³Using the system parameters, one can obtain the group velocity of the probe pulse $V_g \sim 10^{-7}c$. If the time duration of the pulse is $t_0 \sim 10^{-7}$ s, the spatial width of the pulse in the z direction is given by $d_0 \sim V_g t_0 \sim 3 \mu\text{m}$, which is much smaller than the spatial width of $\Delta_d(z)$ ($\sim 10 \mu\text{m}$). This means that during the Fourier transformation, $\Delta_d(z)$ can indeed be approximated as a constant.

i.e., $|\Omega_c|^2 \gg \gamma_{3\alpha}\gamma_{4\alpha}$ ($\alpha = 1, 2$), the Langevin noise terms $\tilde{\mathcal{F}}_{pj}(z, \omega)$ in the envelope equations (9) are very small and hence can be safely neglected [9,54–56].

In the absence of the control field ($\Omega_c = 0$) and the gate atom [$\Delta_d(z) = 0$], the amplitudes of the two polarization components of the probe field (\hat{E}_{p+} and \hat{E}_{p-}) behave in the way of exponential decay with the form $\exp(-\mathcal{D})$ when passing through the atomic medium, with $\mathcal{D} = |g_p|^2 NL/2c\gamma_{31}$ the optical depth (\mathcal{D}) of the atomic gas (which describes the effective coupling strength between the probe field and the atoms). The application of the control field ($\Omega_c \neq 0$) induces deconstructive quantum interference effects for atomic transition paths, so transparent windows on the absorption spectra of the two polarization components will open, resulting in the occurrence of the double Rydberg EIT phenomenon in the system. For completeness, a detailed discussion of the double Rydberg EIT in the absence of the gate atom is given in Appendix C.

III. SWITCH AND PHASE SHIFTS OF PHOTON POLARIZATION QUBITS

A. Rydberg-defect potential for manipulating photon polarization qubits

As illustrated above, the existence of the gate atom contributes the position-dependent detuning $\Delta_d(z)$. In fact, this position-dependent detuning can induce a Rydberg-defect potential for the propagation of the probe pulse. To see this clearly, we write Eq. (9) in the form

$$i\hbar \frac{\partial}{\partial \tau} \tilde{\hat{E}}_{pj}(z, \omega) = V_j(z, \omega) \tilde{\hat{E}}_{pj}(z, \omega), \quad (11)$$

after neglecting the small Langevin noise terms. Here $\tau \equiv ct$ and $V_j(z, \omega) \equiv -\hbar c K_j(z, \omega)$ ($j = +, -$). One can see that $V_+(z, \omega)$ and $V_-(z, \omega)$ play the roles of external potentials for the σ^+ and σ^- polarization components, respectively. It is the z dependence of V_{\pm} that contributes the Rydberg-defect potential to the propagation of the probe pulse and hence induces switch behavior and phase shifts for the photon polarization qubit.

For simplicity, here we discuss in detail only $V_{\pm}(z, \omega)$ near the center point of the EIT transparency windows, i.e., $\omega = 0$. According to (10b) and (10c), we have $V_{\pm}(z, 0) \equiv V_{\pm}(z) = \text{Re}[V_{\pm}(z)] + i\text{Im}[V_{\pm}(z)]$, which means that the Rydberg-defect potential has real and imaginary parts. Detailed expressions of $\text{Re}[V_{\pm}(z)]$ and $\text{Im}[V_{\pm}(z)]$ are presented in Appendix D.

To simplify the expressions of $\text{Re}[V_{\pm}(z)]$ and $\text{Im}[V_{\pm}(z)]$, we note that the decay rates γ_{41} and γ_{42} can be approximated to be zero because the Rydberg state $|4\rangle$ has a long lifetime; moreover, for weak magnetic field B , detunings $\Delta_2 = -\Delta_1 \ll \Delta_d(z)$. Under such a consideration, $\text{Re}[V_{\pm}(z)]$ and $\text{Im}[V_{\pm}(z)]$ can be reduced to the simple forms

$$\begin{aligned} \text{Re}[V_+(z)] &\approx \frac{\mathcal{N}_a \omega_p |\mathbf{e}_{p+} \cdot \mathbf{p}_{31}|^2}{4\epsilon_0} \\ &\times \frac{\Delta_d(z) [|\Omega_c|^2 + (\Delta_3 - \Delta_1)\Delta_d(z)]}{|\Omega_c|^2 + d_{31}\Delta_d(z)^2}, \end{aligned} \quad (12a)$$

$$\begin{aligned} \text{Re}[V_-(z)] &\approx \frac{\mathcal{N}_a \omega_p |\mathbf{e}_{p-} \cdot \mathbf{p}_{32}|^2}{4\epsilon_0} \\ &\times \frac{\Delta_d(z) [|\Omega_c|^2 + (\Delta_3 - \Delta_2)\Delta_d(z)]}{|\Omega_c|^2 + d_{32}\Delta_d(z)^2}, \end{aligned} \quad (12b)$$

$$\text{Im}[V_+(z)] \approx -\frac{\mathcal{N}_a \omega_p |\mathbf{e}_{p+} \cdot \mathbf{p}_{31}|^2}{4\epsilon_0} \frac{\gamma_{31} |\Delta_d(z)|^2}{|\Omega_c|^2 + d_{31}\Delta_d(z)^2}, \quad (12c)$$

$$\text{Im}[V_-(z)] \approx -\frac{\mathcal{N}_a \omega_p |\mathbf{e}_{p-} \cdot \mathbf{p}_{32}|^2}{4\epsilon_0} \frac{\gamma_{32} |\Delta_d(z)|^2}{|\Omega_c|^2 + d_{32}\Delta_d(z)^2}. \quad (12d)$$

From these expressions we see that the Rydberg-defect potentials $V_{\pm}(z) = \text{Re}[V_{\pm}(z)] + i\text{Im}[V_{\pm}(z)]$ are proportional to the position-dependent detuning $\Delta_d(z)$. Figure 2 shows various profiles of the Rydberg-defect potential as functions of z/r_b for different system parameters. The blue solid line and red dashed line in Fig. 2(a) are for the real part $\text{Re}[V_+(z)]$ and the imaginary part $\text{Im}[V_+(z)]$, respectively, by taking $\Delta_3 = \Delta_4 = 0$, $\Omega_c = 2\pi \times 6.37$ MHz, $\mathcal{N}_a = 3 \times 10^{12}$ cm $^{-3}$, and $C_6 = -2\pi \times 625.6$ GHz μm^6 . From the figure we see that $|\text{Im}[V_+(z)]|$ is much larger than $|\text{Re}[V_+(z)]|$. This is due to the selection of vanishing single-photon detuning, i.e., $\Delta_3 = 0$, which makes the system work in a dissipation regime for the propagation of the probe field, useful for designing qubit switches (see Sec. III B below). The result shown by Fig. 2(b) is obtained by using $C_6 = 2\pi \times 625.6$ GHz μm^6 [the other parameters are the same as those in Fig. 2(a)]. In this case the system works still in dissipation propagation regime, i.e., $|\text{Im}[V_+(z)]| \gg |\text{Re}[V_+(z)]|$.

Plotted in Fig. 2(c) are profiles of $\text{Re}[V_+(z)]$ and $\text{Im}[V_+(z)]$ by selecting a large and positive single-photon detuning ($\Delta_3 = 2\pi \times 100$ MHz), with the other system parameters the same as those in Fig. 2(a). One can see that in this situation the real part of the potential is much larger than its imaginary part, i.e., $|\text{Re}[V_+(z)]| \gg |\text{Im}[V_+(z)]|$. This fact tells us that the selection of positive and large single-photon detuning Δ_3 can make the system work in a dispersive regime and $\text{Re}[V_+(z)]$ has the shape of a single barrier (repulsive), useful for realizing large phase shifts for photon qubits (see Sec. III C below). The result given by Fig. 2(d) is obtained by using $\Delta_3 = -2\pi \times 100$ MHz and $C_6 = 2\pi \times 625.6$ GHz μm^6 , with the other parameters the same as those in Fig. 2(a). In this case, the system works still in dispersion regime, but $\text{Re}[V_+(z)]$ displays the shape of single well. This means that the Rydberg-defect potential of this case can be used to trap the photon polarization qubit, which is interesting but will not be discussed in the present work.

Note that, by inspecting the symmetry of the excitation configuration of the double Rydberg EIT [see the left part of Fig. 1(a)], we have $V_-(z) \approx V_+(z)$. Thus the profile of the Rydberg-defect potential $V_-(z)$ is basically the same as that of $V_+(z)$. This point can be seen clearly from the expressions (12a)–(12d).

Based on the above analysis, we see that the dispersion coefficient of the Rydberg-Rydberg interaction C_6 and the single-photon detuning Δ_3 are two important parameters for controlling the property of the Rydberg-defect potential.

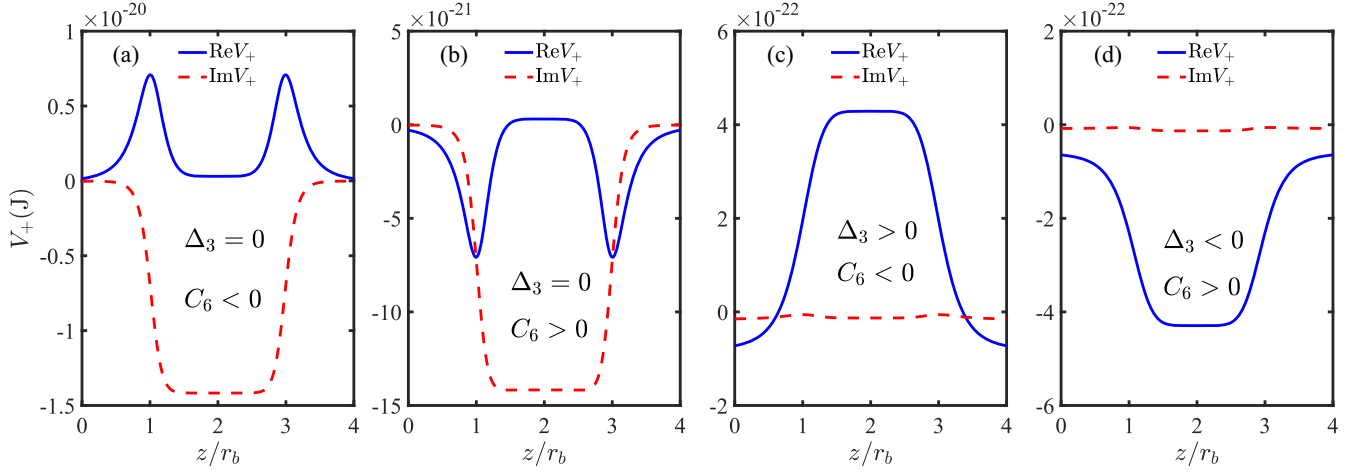


FIG. 2. Rydberg-defect potential $V_+(z) = \text{Re}[V_+(z)] + i \text{Im}[V_+(z)]$. (a) The blue solid line and red dashed line are the real part $\text{Re}[V_+(z)]$ and the imaginary part $\text{Im}[V_+(z)]$, respectively, as a function of z/r_b , by taking $\Delta_3 = \Delta_4 = 0$, $\Omega_c = 2\pi \times 6.37 \text{ MHz}$, $\mathcal{N}_a = 3 \times 10^{12} \text{ cm}^{-3}$, and $C_6 = -2\pi \times 625.6 \text{ GHz } \mu\text{m}^6$. The system works in a dissipation regime for the propagation of the probe pulse, useful for designing qubit switches. (b) Same as (a) but for $C_6 = 2\pi \times 625.6 \text{ GHz } \mu\text{m}^6$. (c) Same as (a) but with $\Delta_3 = 2\pi \times 100 \text{ MHz}$. The system works in a dispersion regime for the propagation of the probe pulse, useful for realizing large phase shifts for photon qubits. (d) Same as (a) but with $\Delta_3 = -2\pi \times 100 \text{ MHz}$ and $C_6 = 2\pi \times 625.6 \text{ GHz } \mu\text{m}^6$. Due to the symmetry of the excitation configuration of the double Rydberg EIT, $V_-(z) \approx V_+(z)$, and thus is not shown.

Based on such results, we can realize various Rydberg-defect potentials and hence can actively manipulate the behavior of the incident photon polarization qubits. In the following discussion, we consider only two cases for $C_6 < 0$, i.e., the Rydberg-defect potentials of the forms shown in Figs. 2(a) and 2(c).

B. Switch of the photon polarization qubits in the dissipation regime

We now explore the possibility of different type of photon switch in the system. Single photon switches are optical devices for controlling the transmission of target photons through the application only a single gate photon. They are key devices for all-optical quantum information processing [57]. One of techniques for building single-photon switches is the use of the dissipative optical nonlinearity via Rydberg EIT. In the past few years, the possibility of realizing such switches for target photons with one polarization component has been demonstrated experimentally [35–38]. Here we show that the model proposed above can be used to realize another type of single-photon switch, which is for the single photon with two polarization components, i.e., a photon polarization qubit switch. The basic idea of the scheme is the following. First, a single gate photon is stored in the Rydberg state $|3\rangle_g$ [as shown in the right part of Fig. 1(a)], which provides the Rydberg-defect potential discussed in the preceding section. Second, a probe photon qubit (as a target photon) with σ^+ and σ^- polarization components is incident into the atomic gas working in the dissipation regime of the double Rydberg EIT (realized by taking zero single-photon detuning, i.e., $\Delta_3 = 0$), for which the imaginary part of the Rydberg-defect potential is much bigger than its real part [see Fig. 2(a)]. When the gate photon is absent, the photon polarization qubit would propagate in the atomic gas nearly without absorption

[as schematically shown in the top of Fig. 1(c)]; however, when the gate photon is present, the strong Rydberg-Rydberg interaction between the states $|4\rangle$ and $|3\rangle_g$ results in a Rydberg blockade effect (the breaking of the double Rydberg EIT) and hence switches the atomic gas from highly transparent to strongly absorptive [as shown in the middle of Fig. 1(c)].

To this end, we consider the dynamics of the two polarization components of the probe pulse in the presence of the Rydberg-defect potential, which is controlled by the envelope equation (9). By directly integrating Eq. (9) from 0 to L , we get the solution (in the frequency domain)

$$\tilde{E}_{pj}(L, \omega) = \tilde{E}_{pj}(0, \omega) \exp\left(i \int_0^L dz K_j(z, \omega)\right), \quad (13)$$

with $j = +, -$. The solution in time domain can be obtained by using the inverse Fourier transformation, which reads

$$\hat{E}_{pj}(L, t) = \int_{-\infty}^{+\infty} d\omega \tilde{E}_{pj}(0, \omega) \times \exp\left[i \int_0^L dz K_j(z, \omega) - i\omega\left(t - \frac{L}{c}\right)\right]. \quad (14)$$

Here $\tilde{E}_{pj}(0, \omega)$ is the Fourier transform of $\hat{E}_{pj}(z, t)$ at the input boundary $z = 0$. Since the probe field is a pulse, $\tilde{E}_{pj}(0, \omega)$ is narrow in ω and hence we can expand $K_j(z, \omega)$ near $\omega = 0$, i.e., $K_j(z, \omega) = K_{0j} + \omega K_{1j} + \dots$, with $K_{0j} \equiv K_j(z, \omega)|_{\omega=0}$ and $K_{1j} \equiv (\partial K_j / \partial \omega)|_{\omega=0}$. Then (14) can be reduced to the form

$$\hat{E}_{pj}(L, t) \approx \hat{E}_{pj}(0, t - L'/V_{gj}) e^{-\eta_j + i\phi_j}, \quad (15)$$

where

$$\phi_+ = \frac{|g_p|^2 N}{c} \operatorname{Re} \left(\int_0^L dz a_{31}(z) \right), \quad (16a)$$

$$\phi_- = \frac{|g_p|^2 N}{c} \operatorname{Re} \left(\int_0^L dz a_{32}(z) \right), \quad (16b)$$

$$\eta_+ = \frac{|g_p|^2 N}{c} \operatorname{Im} \left(\int_0^L dz a_{31}(z) \right), \quad (16c)$$

$$\eta_- = \frac{|g_p|^2 N}{c} \operatorname{Im} \left(\int_0^L dz a_{32}(z) \right), \quad (16d)$$

$$L' = L - 2r_b \approx L, \quad (16e)$$

with

$$a_{31}(z) = \frac{d_{41} - \Delta_d(z)}{2\{|\Omega_c|^2 - d_{31}[d_{41} - \Delta_d(z)]\}}, \quad (17a)$$

$$a_{32}(z) = \frac{d_{42} - \Delta_d(z)}{2\{|\Omega_c|^2 - d_{32}[d_{42} - \Delta_d(z)]\}}. \quad (17b)$$

In these expressions, L' is the reduced medium length due to the existence of the Rydberg blockade and $V_{gj} = [K_{1j}]^{-1} \equiv [(\partial K_j / \partial \omega)|_{\omega=0}]^{-1}$ is the group velocity of the j th polarization component, which is a constant after the pulse passes over the gate atom. Using the system parameters given in Sec. II A and taking $\mathcal{N}_a = 3 \times 10^{12} \text{ cm}^{-3}$ and $\Omega_c = 2\pi \times 6.37 \text{ MHz}$, we obtain $V_{g-} \approx V_{g+} = 6.46 \times 10^{-7} c$, i.e., the probe pulse is a slow-light qubit.

The dynamics of the incident photon polarization qubit under the action of the Rydberg-defect potential is characterized by key quantities η_j and ϕ_j ($j = +, -$) in the solution (15), which describe the amplitude attenuations and phase shifts of the two polarization components after traversing the gate atom, respectively. To demonstrate this, we first consider the switch behavior of the photon polarization qubit by assuming that the system works in the dissipation regime of the double Rydberg EIT, i.e., $\Delta_3 = 0$.

Figure 3(a) shows the numerical result for the qubit switch. The red dashed line in the figure is the amplitude attenuation factor η_+ for the σ^+ polarization component [using the expression given by (16c)], plotted as a function of optical depth \mathcal{D} . The phase shift ϕ_+ in this regime is also displayed by the blue solid line. The result is obtained for cold ^{85}Rb atomic gas, by taking $B = 1.5 \text{ G}$ (i.e., $\Delta_2 = -\Delta_1 = 2\pi \times 0.7 \text{ MHz}$), $\Delta_4 = 0$, and the other system parameters the same as in Sec. II A.⁴ The inset of the figure gives the shape of the Rydberg-defect potential [the same as Fig. 2(a)]. Since in double Rydberg EIT there exists a configuration symmetry for excitation paths of the σ^+ and σ^- polarization components, the amplitude attenuation factor η_- and phase shift ϕ_- for the σ^- component have behaviors similar to those for η_+ and ϕ_+ , respectively, and thus are omitted here.

From the figure we see that η_+ reaches the value 1 when $\mathcal{D} \approx 15$ and it grows rapidly as \mathcal{D} is increased further. This fact tells us that, because of the rapid exponential attenuation

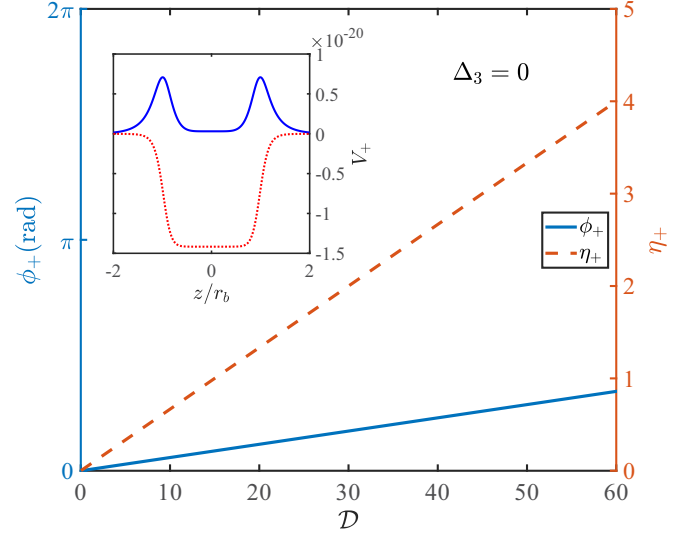


FIG. 3. Switch of the photon polarization qubit in the dissipation regime of the double Rydberg EIT ($\Delta_3 = 0$). The red dashed line is the amplitude attenuation factor η_+ for the σ^+ polarization component, as a function of optical depth $\mathcal{D} \equiv |g_p|^2 NL / 2c\gamma_{31}$. Here η_+ reaches value 1 at $\mathcal{D} \approx 15$; it grows rapidly as \mathcal{D} is increased further. The phase shift ϕ_+ in this regime is also shown by the blue solid line. The inset shows the shape of the Rydberg-defect potential V_+ . Because of the rapid exponential attenuation of the amplitude of the incident photon, the system acts as a well-behaved photon qubit switch. Due to the excitation configuration symmetry of the double Rydberg EIT, the behaviors of the amplitude attenuation factor η_- and the phase shift ϕ_- for the σ^- component are similar to those of the σ^+ component and hence are not shown.

of the incident photon amplitude, the stored gate photon can act indeed as a well-behaved single-photon switch, which can significantly impede the transmission of the incident photon polarization qubit [as shown by the middle part of Fig. 1(c)].

C. Phase shifts of the photon polarization qubit in the dispersion regime

We now turn to consider how to get large phase shifts for the photon polarization qubit. It is known that the strong dispersive interaction between the gate photon and target photon can be used to access a significant phase shift for the target photon, which is also important for all-optical quantum information processing [3,6,9,31,32,39,41,43,44,58]. Here we show that large phase shifts for the two polarization components of the incident photon polarization qubit can be acquired under the action of the gate photon if the system works in the dispersion regime of the double Rydberg EIT.

The one-photon detuning Δ_3 is a key parameter to control the dissipation and dispersion behaviors of the system. When $|\Delta_3| \gg \gamma_{31}$, the system works in the dispersion regime. Note that the general solution of the envelope equation (9), given by (15), together with (16) and (17), is valid for any value of the one-photon detuning Δ_3 . It thus can also be used to calculate the phase shifts ϕ_j and amplitude attenuation factors η_j ($j = +, -$) of the photon polarization qubit for nonzero Δ_3 .

⁴Since γ_{41} and γ_{42} are much smaller than $\Delta_d(z)$, the contributions to the amplitude attenuations and phase shifts by d_{41} and d_{42} in (17a) and (17b) are negligible.

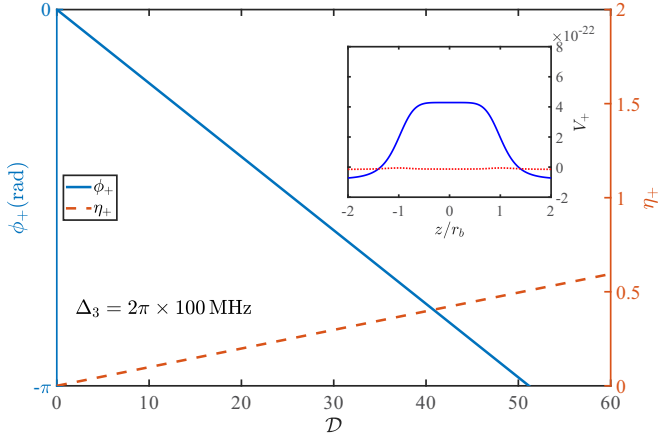


FIG. 4. Phase shift of the photon polarization qubit in the dispersion regime for the σ^+ component (with $\Delta_3 = 2\pi \times 100$ MHz and $B = 1.5$ G). The blue solid line is for ϕ_+ , as a function of optical depth \mathcal{D} . Here ϕ_+ reaches $-\pi$ rad for $\mathcal{D} \approx 51$; it can be increased further as \mathcal{D} increases. The red dashed line shows η_+ , which is considered to be small in the range of $\mathcal{D} \leq 51$ because the optical absorption is suppressed in this regime. The inset shows the shape of the Rydberg-defect potential V_+ .

Shown in Fig. 4 is the numerical result for the σ^+ polarization component in the dispersion regime ($\Delta_3 = 2\pi \times 100$ MHz). The blue solid line in the figure is the phase shift ϕ_+ as a function of optical depth \mathcal{D} . The result is obtained still for the cold ^{85}Rb atomic gas, with $B = 1.5$ G (i.e., $\Delta_2 = -\Delta_1 = 2\pi \times 0.7$ MHz), $\Delta_4 = 0$, and the other parameters given in Sec. II A. The inset of the figure gives the shape of the Rydberg-defect potential [i.e., Fig. 2(c)]. The plot in Fig. 5 is similar to that in Fig. 4 but for ϕ_- and η_- of the σ^- component. For large Δ_3 and nonzero B , the symmetry of the two Rydberg EITs for the σ^+ and σ^- polarization

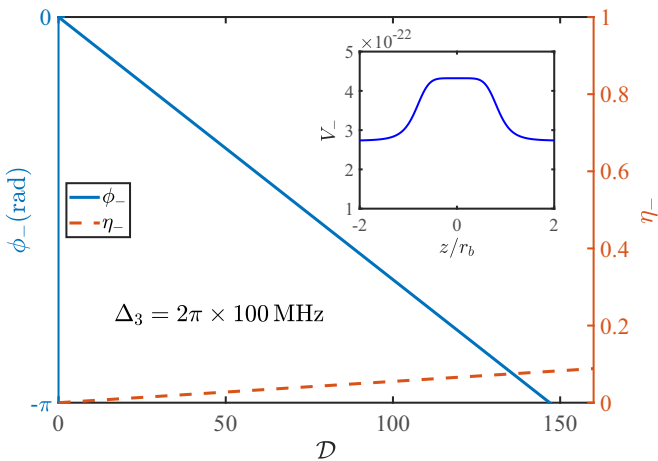


FIG. 5. Phase shift of the photon polarization qubit in the dispersion regime for the σ^- component (with $\Delta_3 = 2\pi \times 100$ MHz and $B = 1.5$ G). The blue solid line is for ϕ_- as a function of optical depth \mathcal{D} . Here ϕ_- reaches $-\pi$ rad for $\mathcal{D} \approx 146$; it can be increased further as \mathcal{D} increases. The red dashed line shows η_- , which is much smaller than η_+ because the optical absorption is greatly suppressed in this regime. The inset shows the shape of the Rydberg-defect potential V_- .

components, respectively, is broken and hence the phase shift ϕ_- and the amplitude attenuation factor η_- for the σ^- polarization component have different behavior than those of the σ^+ component.

From Fig. 4 we see that ϕ_+ reaches the value $-\pi$ rad for $\mathcal{D} \approx 51$ and it increases further as \mathcal{D} is increased. The amplitude attenuation factors η_+ is also shown by the red dashed line; it is very small due to the large Δ_3 , by which the photon absorption is greatly suppressed. From Fig. 5 one can see that although ϕ_- behaves similarly to ϕ_+ , a large optical depth ($\mathcal{D} \approx 146$) is needed to reach the value of $-\pi$. In addition, η_- is much smaller than η_+ , which can be seen by comparing Fig. 5 with Fig. 4.

Consequently, due to the existence of the Rydberg-defect potential contributed by the stored gate photon, in the dispersion regime the two polarization components of the incident single-photon qubit can indeed acquire significant phase shifts with a very small attenuation of qubit amplitude. However, these two polarization components display different behaviors due to large one-photon detuning Δ_3 and the existence of a nonzero magnetic field B .

D. Propagation of the qubit wave packet

To be more intuitive, we now present a study of the propagation of the photon polarization qubit when it passes through the Rydberg defect (gate atom) using the Schrödinger picture. In such an approach, the qubit can be described by a single-photon wave packet with two polarization components.

Since the input probe pulse is in a single-photon qubit state, in the atomic medium the photon state takes the form

$$\begin{aligned} |\Phi(t)\rangle &= |\Phi_+(t)\rangle + |\Phi_-(t)\rangle \\ &= \int dz [\Phi_+(z, t) \hat{E}_{p+}^\dagger(z) + \Phi_-(z, t) \hat{E}_{p-}^\dagger(z)] |0\rangle. \end{aligned} \quad (18)$$

Here $|0\rangle$ is electromagnetic vacuum and $\Phi_j(z, t) \equiv \langle 0 | \hat{E}_{pj}(z) | \Phi_j(t) \rangle$ is the effective wave function of the j th polarization component ($j = +, -$), obeying the normalization condition $\int dz [|\Phi_+(z, t)|^2 + |\Phi_-(z, t)|^2] = 1$.

Based on Eq. (9) and the above definition of the one-photon state vector, it is easy to derive the equation

$$i \frac{\partial}{\partial z} \tilde{\Phi}_j(z, \omega) + K_j(z, \omega) \tilde{\Phi}_j(z, \omega) = 0, \quad (19)$$

where $\tilde{\Phi}_j(z, \omega) \equiv (1/\sqrt{2\pi}) \int_{-\infty}^{\infty} dt \Phi_j(z, t) e^{i\omega t}$ is the Fourier transform of $\Phi_j(z, t)$ ($j = +, -$). We assume that the j th component of the incident single-photon wave packet has the Gaussian form

$$\Phi_j(0, t) = \sqrt{A_j} \sqrt{\frac{2\sqrt{\ln(2)}}{t_0\sqrt{\pi}}} \exp\left(-2\ln(2)\frac{t^2}{t_0^2}\right), \quad (20)$$

where A_j are amplitudes satisfying $A_+ + A_- = 1$ and t_0 is the full width at half maximum (FWHM) of $|\Phi_j(0, t)|^2$. The Fourier transform of $\Phi_j(0, t)$ reads

$$\tilde{\Phi}_j(0, \omega) = \sqrt{A_j} \sqrt{\frac{2\sqrt{\ln(2)}}{\omega_0\sqrt{\pi}}} \exp\left(-2\ln(2)\frac{\omega^2}{\omega_0^2}\right), \quad (21)$$

where $\omega_0 = 4\ln(2)/t_0$ is the FWHM of $|\tilde{\Phi}_j(0, \omega)|^2$.

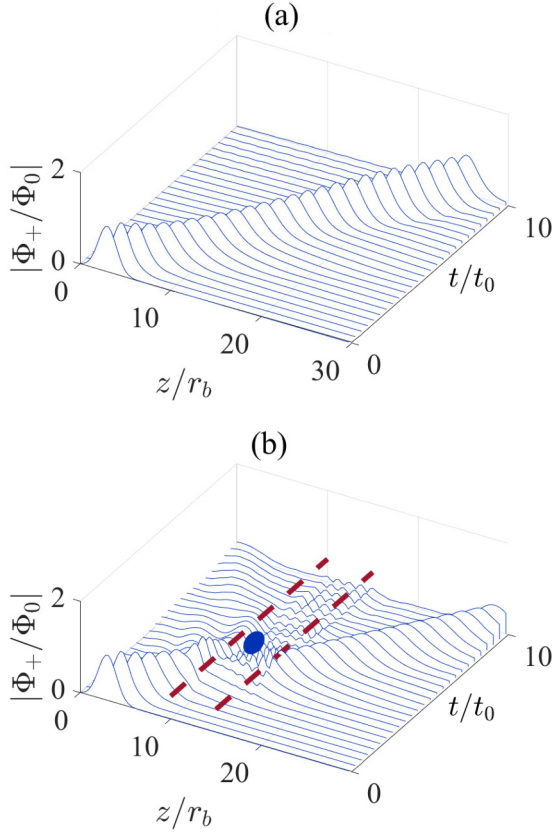


FIG. 6. Propagation of the wave packet Φ_+ of the σ^+ polarization component in the dispersion regime of the double Rydberg EIT ($\Delta_3 = 2\pi \times 100$ MHz and $B = 1.5$ G). (a) Plot of Φ_+ as a function of time t and position z in the absence of the gate photon. Here Φ_0 represents the initial amplitude of Φ_+ . (b) Same as (a) but in the presence of the gate photon. The width of the Rydberg-defect potential is marked by two red dashed lines; the gate atom is denoted by the blue circle.

By solving Eq. (19) under the boundary condition (21), we can obtain $\Phi_j(z, t)$ through the relation $\Phi_j(z, t) = (1/\sqrt{2\pi}) \int_{-\infty}^{\infty} d\omega \tilde{\Phi}_j(z, \omega) e^{-i\omega t}$. Figure 6(a) shows Φ_+ of the σ^+ polarization component as a function of time t and spatial coordinate z for the case of no gate photon, with $\Phi_0 = [2\sqrt{\ln(2)} A_j / t_0 \sqrt{\pi}]^{1/2}$ representing the initial amplitude of Φ_+ . When plotting the figure, we have chosen $\Delta_3 = 2\pi \times 100$ MHz, $B = 1.5$ G, $t_0 = 1 \times 10^{-7}$ s, $A_+ = \frac{1}{2}$, and $\mathcal{N}_a = 3 \times 10^{12}$ cm $^{-3}$. We see that the wave packet propagates quite stably. The reason is that, in the absence of the gate atom, the phase shift and attenuation of the wave packet are nearly vanishing due to the EIT effect.

Plotted in Fig. 6(b) is the wave function Φ_+ as a function of t and z in the presence of the gate photon, with the system parameters the same as those used in Fig. 6(a). In the figure, the width of the Rydberg-defect potential is indicated by the two red dashed lines and the gate atom is denoted by the blue circle. For comparison, Fig. 7 shows the propagation of the wave packet Φ_- of the σ^- polarization component. We see that in the presence of the gate atom Φ_- displays behavior a little different from that of Φ_+ .

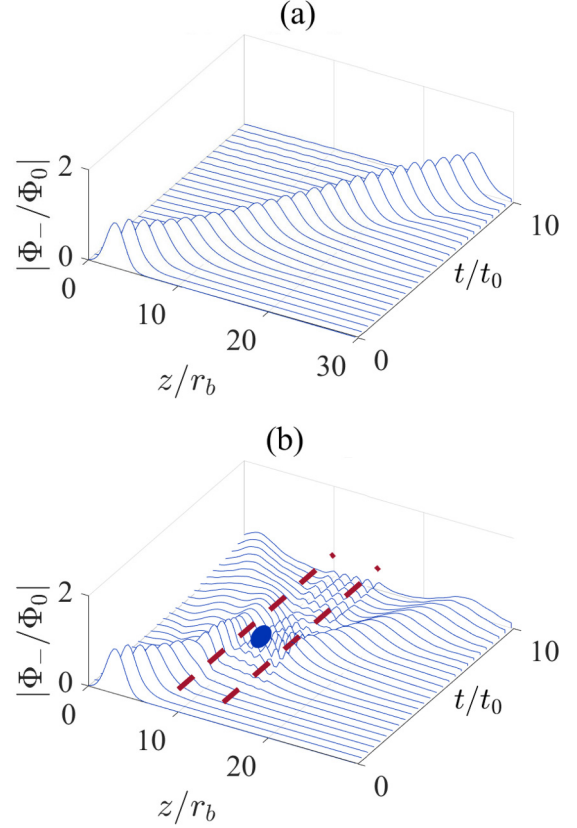


FIG. 7. Propagation of the wave packet Φ_- of the σ^- polarization component in the dispersion regime of the double Rydberg EIT ($\Delta_3 = 2\pi \times 100$ MHz and $B = 1.5$ G). (a) Wave function Φ_- as a function of time t and position z in the absence of the gate photon. Here Φ_0 represents the initial amplitude of Φ_- . (b) Same as (a) but in the presence of the gate photon. The width of the Rydberg-defect potential is marked by two red dashed lines; the gate atom is denoted by the blue circle.

If the photon polarization qubit is incident to the atomic gas at $(z, t) = (0, 0)$, the state vector of the probe field for this input state reads $|\Phi_{+,in}(0)\rangle = c_+ |\sigma^+\rangle + c_- |\sigma^-\rangle$, with $c_+ = \Phi_{+,in}(0, 0)$, $c_- = \Phi_{-,in}(0, 0)$, $|\sigma^+\rangle = \hat{E}_{p+}^\dagger(0)|0\rangle$, and $|\sigma^-\rangle = \hat{E}_{p-}^\dagger(0)|0\rangle$. Depending on whether no or one gate photon is stored, the output qubit state (after passing through the atomic medium) is given by

$$|\Phi_{out,0}\rangle \propto (c_+ |\sigma^+\rangle + c_- |\sigma^-\rangle) \otimes |0\rangle_g, \quad (22a)$$

$$|\Phi_{out,1}\rangle \propto (c_+ e^{-\eta_+} e^{i\phi_+} |\sigma^+\rangle + c_- e^{-\eta_-} e^{i\phi_-} |\sigma^-\rangle) \otimes |1\rangle_g. \quad (22b)$$

Here $|1\rangle_g$ ($|0\rangle_g$) is the Fock state with one gate photon (no gate photon) stored in the Rydberg state $|3\rangle_g$ and η_j and ϕ_j are the amplitude attenuation factors and the phase shifts for the j th polarization component ($j = +, -$), respectively, given by (16a)–(16d).

E. Magnetic-field-induced switching behavior of the photon polarization qubit

How to detect weak magnetic fields is an important topic in the study of precision measurements [59]. As the final

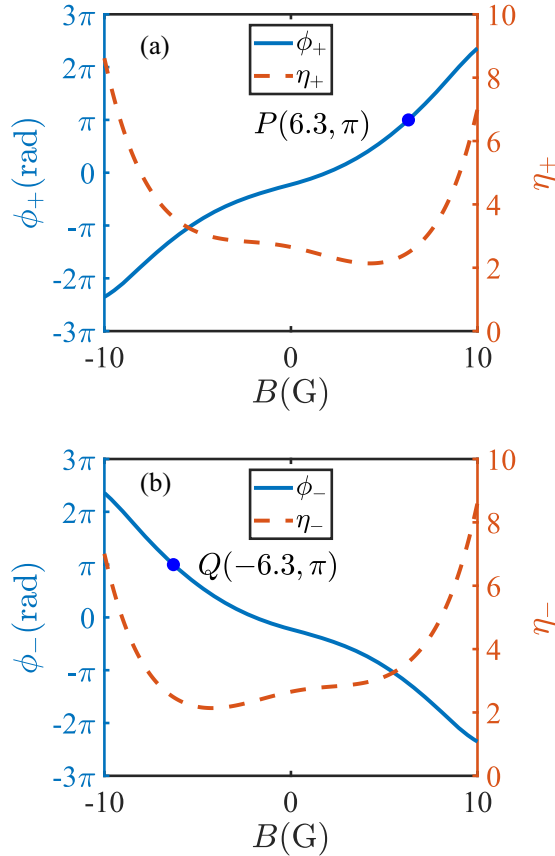


FIG. 8. Magnetic-field-induced switching behavior of the photon polarization qubit. (a) Amplitude attenuation factor η_+ (red dashed line) and phase shift ϕ_+ (blue solid line) as functions of magnetic field B , for $\Delta_3 = 0$, $\mathcal{N}_a = 3 \times 10^{12} \text{ cm}^{-3}$, and $L = 50 \mu\text{m}$. Here $P(6.3, \pi)$ (blue circle) means the numerical point with $B = 6.3 \text{ G}$ and $\phi_+ = \pi$. (b) Same as (a) but for the amplitude attenuation factor η_- (red dashed line) and phase shift ϕ_- (blue solid line). Here $Q(-6.3, \pi)$ (blue circle) means the numerical point with $B = -6.3 \text{ G}$ and $\phi_- = \pi$.

example, here we consider another possible application of the strong interaction between the gate photon and the photon polarization qubit. We demonstrate that the present system can be used to design a different type of magnetometer that can be used to detect weak magnetic fields.

As indicated at the end of Sec. II A, when the magnetic field $\mathbf{B} = (0, 0, B)$ is applied to the system the Zeeman effect induced by the magnetic field makes the two degenerate levels $|1\rangle$ and $|2\rangle$ produce a level splitting proportional to B . Since B is contained in the HM equations (6) and (7), solutions of the amplitude attenuation factors η_j and phase shifts ϕ_j ($j = +, -$), given by (16a)–(16d), are also B dependent. Hence, the behaviors of the switch and phase shift of the photon polarization qubit can display a dependence on B .

Figures 8(a) and 8(b) show the amplitude attenuation factors η_j (red dashed lines) and phase shifts ϕ_j (blue solid lines) for the j th polarization component ($j = +, -$), plotted as functions of the magnetic field B , by taking the system parameters to be $\Delta_3 = 0$, $\mathcal{N}_a = 3 \times 10^{12} \text{ cm}^{-3}$, and $L = 50 \mu\text{m}$. The point $P(6.3, \pi)$ (blue circle) in Fig. 8(a) is the one for $B = 6.3 \text{ G}$ and $\phi_+ = \pi$, while the point $Q(-6.3, \pi)$ in Fig. 8(b)

is the one for $B = -6.3 \text{ G}$ and $\phi_- = \pi$. From these results we see that both η_j and ϕ_j are very sensitive to B . Thereby, the present system can be used to design a magnetometer to detect the external magnetic field B , which can be realized by measuring the amplitude attenuation factors η_j and/or phase shifts ϕ_j of the photon polarization qubit.

IV. CONCLUSION

The calculation results given above are based on the assumption that the gate atom is located at the fixed position $z = z_g$. To be rigorous and realistic, the derivation of the above results by the influence of gate-atom delocalization (which may be due to the intrinsic quantum motion of the gate atom and as well as other possible noise acting on the atom) should be estimated. To this end, we assumed that the gate atom may randomly occupy different spatial positions around z_g , with the density described by $\rho_g(z'_g, \xi) = f(\xi)\delta[z'_g - (z_g + \xi)]$. Here $f(\xi) \equiv (1/\sqrt{\pi}\sigma)\exp[-(\xi/\sigma)^2]$ is the normalized distribution function, with σ the distribution width and ξ the random variable describing the derivation of the gate-atom position relative to z_g . Based on such a random density distribution, we have carried out a numerical simulation on the topics described above, with the result presented in Appendix E. The simulation shows that the gate-atom delocalization does not significantly modify the main conclusions given above, which means that the single-photon qubit switch, phase shifts, and weak-magnetic-field measurement can still be achieved in the system.

In conclusion, in this article we have suggested and analyzed a scheme for manipulating the propagation of single-photon pulses of two polarization components in a cold atomic gas via double Rydberg EIT. Through solving the Heisenberg-Maxwell equations governing the quantum dynamics of the atoms and quantized probe field, we have shown that, by storing a gate photon in a Rydberg state, a deep and adjustable optical potential for photon polarization qubits can be realized based on the strong Rydberg-Rydberg interaction. We have also shown that this scheme can be utilized to design all-optical switches of photon polarization qubits in the dissipative propagation regime and generate large phase shifts to them in the dispersive propagation regime. Furthermore, we have demonstrated that such a scheme can be employed to detect weak magnetic fields that induce the Zeeman splitting of the atomic levels.

The theoretical approach developed here can be generalized to the study of all-optical transistors and phase gates of photon qubits and qudits based on Rydberg atoms. The results reported in this work are useful not only for the understanding of the quantum optical property of Rydberg atomic gases, but also for the design of quantum devices at the single-photon level, which are promising in applications for quantum information processing.

ACKNOWLEDGMENT

The authors thank Zhengyang Bai and Jingzhong Zhu for useful discussions. This work was supported by the National Natural Science Foundation of China under Grant No. 11975098.

APPENDIX A: EXPLICIT EXPRESSION OF THE HEISENBERG EQUATION OF MOTION (6)

The explicit expression of the Heisenberg equation of motion (6) for atomic operators is given by

$$i\left(\frac{\partial}{\partial t} + \Gamma_{21}\right)\hat{S}_{11} - i\Gamma_{12}\hat{S}_{22} - i\Gamma_{13}\hat{S}_{33} + g_{p+}^*\hat{E}_{p+}^\dagger\hat{S}_{31} - g_{p+}\hat{S}_{13}\hat{E}_{p+} - i\hat{F}_{11} = 0, \quad (\text{A1a})$$

$$i\left(\frac{\partial}{\partial t} + \Gamma_{12}\right)\hat{S}_{22} - i\Gamma_{21}\hat{S}_{11} - i\Gamma_{23}\hat{S}_{33} + g_{p-}^*\hat{E}_{p-}^\dagger\hat{S}_{32} - g_{p-}\hat{S}_{23}\hat{E}_{p-} - i\hat{F}_{22} = 0, \quad (\text{A1b})$$

$$i\left(\frac{\partial}{\partial t} + \Gamma_3\right)\hat{S}_{33} - i\Gamma_{34}\hat{S}_{44} - g_{p+}^*\hat{E}_{p+}^\dagger\hat{S}_{31} + g_{p+}\hat{E}_{p+}\hat{S}_{13} - g_{p-}^*\hat{E}_{p-}^\dagger\hat{S}_{32} + g_{p-}\hat{S}_{23}\hat{E}_{p-} + \Omega_c^*\hat{S}_{43} - \Omega_c\hat{S}_{34} - i\hat{F}_{33} = 0, \quad (\text{A1c})$$

$$i\left(\frac{\partial}{\partial t} + \Gamma_{34}\right)\hat{S}_{44} - \Omega_c^*\hat{S}_{43} + \Omega_c\hat{S}_{34} - i\hat{F}_{44} = 0, \quad (\text{A1d})$$

$$\left(i\frac{\partial}{\partial t} + d_{21}\right)\hat{S}_{21} + g_{p-}^*\hat{E}_{p-}^\dagger\hat{S}_{31} - g_{p+}\hat{S}_{23}\hat{E}_{p+} - i\hat{F}_{21} = 0, \quad (\text{A1e})$$

$$\left(i\frac{\partial}{\partial t} + d_{31}\right)\hat{S}_{31} + \Omega_c^*\hat{S}_{41} + g_{p+}(\hat{S}_{11} - \hat{S}_{33})\hat{E}_{p+} + g_{p-}\hat{S}_{21}\hat{E}_{p-} - i\hat{F}_{31} = 0, \quad (\text{A1f})$$

$$\left(i\frac{\partial}{\partial t} + d_{32}\right)\hat{S}_{32} + \Omega_c^*\hat{S}_{42} + g_{p-}(\hat{S}_{22} - \hat{S}_{33})\hat{E}_{p-} + g_{p+}\hat{S}_{12}\hat{E}_{p+} - i\hat{F}_{32} = 0, \quad (\text{A1g})$$

$$\left(i\frac{\partial}{\partial t} + d_{41} - \Delta_d(z)\right)\hat{S}_{41} + \Omega_c\hat{S}_{31} - g_{p+}\hat{S}_{43}\hat{E}_{p+} - i\hat{F}_{41} = 0, \quad (\text{A1h})$$

$$\left(i\frac{\partial}{\partial t} + d_{42} - \Delta_d(z)\right)\hat{S}_{42} + \Omega_c\hat{S}_{32} - g_{p-}\hat{S}_{43}\hat{E}_{p-} - i\hat{F}_{42} = 0, \quad (\text{A1i})$$

$$\left(i\frac{\partial}{\partial t} + d_{43} - \Delta_d(z)\right)\hat{S}_{43} + \Omega_c(\hat{S}_{33} - \hat{S}_{44}) - g_{p+}^*\hat{E}_{p+}^\dagger\hat{S}_{41} - g_{p-}^*\hat{E}_{p-}^\dagger\hat{S}_{42} - i\hat{F}_{43} = 0. \quad (\text{A1j})$$

Here $d_{\alpha\beta} = \Delta_\alpha - \Delta_\beta + i\gamma_{\alpha\beta}$ ($\alpha \neq \beta$), $\gamma_{\alpha\beta} \equiv (\Gamma_\alpha + \Gamma_\beta)/2 + \gamma_{\alpha\beta}^{\text{dep}}$, and $\Gamma_\beta \equiv \sum_{\alpha < \beta} \Gamma_{\alpha\beta}$, with $\Gamma_{\alpha\beta}$ the decay rate of the spontaneous emission from the state $|\beta\rangle$ to the state $|\alpha\rangle$ and $\gamma_{\alpha\beta}^{\text{dep}}$ the dephasing rate between $|\alpha\rangle$ and $|\beta\rangle$. The half Rabi frequency of the control field is defined as $\Omega_c \equiv (\mathbf{e}_c \cdot \mathbf{p}_{43})\mathcal{E}_c/\hbar$.

APPENDIX B: DERIVATION OF THE TWO-COMPONENT ENVELOPE EQUATIONS OF THE PROBE FIELD

The dynamical evolution of the probe field is controlled by the HM equations (6) and (7). Because we are interested in the case of the probe field at the single-photon level, the nonlinear terms in the HM equations play no significant role and hence can be safely disregarded. Based on this idea, we take $\hat{S}_{\alpha\beta} \rightarrow S_{\alpha\beta}^{(0)} + \hat{S}_{\alpha\beta}$, with $S_{\alpha\beta}^{(0)}$ the steady-state solution of $\hat{S}_{\alpha\beta}$ in the absence of the probe field, i.e., $S_{11}^{(0)} = S_{22}^{(0)} = \frac{1}{2}$, and otherwise $S_{\alpha\beta}^{(0)} = 0$. Then, by taking $\hat{S}_{\alpha\beta}$ and \hat{E}_{pj} as small quantities, Eqs. (6) and (7) are reduced to

$$\left(i\frac{\partial}{\partial t} + d_{31}\right)\hat{S}_{31} + \Omega_c^*\hat{S}_{41} + \frac{g_{p+}\hat{E}_{p+}}{2} - i\hat{F}_{31} = 0, \quad (\text{B1a})$$

$$\left(i\frac{\partial}{\partial t} + d_{32}\right)\hat{S}_{32} + \Omega_c^*\hat{S}_{42} + \frac{g_{p-}\hat{E}_{p-}}{2} - i\hat{F}_{32} = 0, \quad (\text{B1b})$$

$$\left(i\frac{\partial}{\partial t} + d_{41} - \Delta_d(z)\right)\hat{S}_{41} + \Omega_c\hat{S}_{31} - i\hat{F}_{41} = 0, \quad (\text{B1c})$$

$$\left(i\frac{\partial}{\partial t} + d_{42} - \Delta_d(z)\right)\hat{S}_{42} + \Omega_c\hat{S}_{32} - i\hat{F}_{42} = 0, \quad (\text{B1d})$$

$$i\left(\frac{\partial}{\partial z} + \frac{1}{c}\frac{\partial}{\partial t}\right)\hat{E}_{p+} + \frac{g_{p+}^*N}{c}\hat{S}_{31} = 0, \quad (\text{B1e})$$

$$\left(\frac{\partial}{\partial z} + \frac{1}{c}\frac{\partial}{\partial t}\right)\hat{E}_{p-} + \frac{g_{p-}^*N}{c}\hat{S}_{32} = 0. \quad (\text{B1f})$$

Since these equations are linear, they can be solved easily by using the Fourier transform

$$\hat{X}(z, t) = \frac{1}{\sqrt{2\pi}} \int_{-\infty}^{+\infty} d\omega \tilde{X}(z, \omega) e^{-i\omega t}, \quad (\text{B2a})$$

$$\tilde{X}(z, \omega) = \frac{1}{\sqrt{2\pi}} \int_{-\infty}^{+\infty} dt \hat{X}(z, t) e^{i\omega t}, \quad (\text{B2b})$$

where \hat{X} denotes \hat{S}_{31} , \hat{S}_{32} , \hat{S}_{41} , \hat{S}_{42} , \hat{F}_{31} , \hat{F}_{32} , \hat{F}_{41} , \hat{F}_{42} , and \hat{E}_{pj} ($j = +, -$). Substituting (B2) into (B1a)–(B1d), we get the atomic transition operators expressed by the polarization components of the probe field

$$\tilde{S}_{31} = \frac{Y_1(\omega)}{2D_1(\omega)} g_{p+} \tilde{E}_{p+} - i \frac{Y_1(\omega) \tilde{F}_{31} - \Omega_c \tilde{F}_{41}}{D_1(\omega)}, \quad (\text{B3a})$$

$$\tilde{S}_{32} = \frac{Y_2(\omega)}{2D_2(\omega)} g_{p-} \tilde{E}_{p-} - i \frac{Y_2(\omega) \tilde{F}_{32} - \Omega_c \tilde{F}_{42}}{D_2(\omega)}, \quad (\text{B3b})$$

$$\tilde{S}_{41} = \frac{-\Omega_c}{2D_1(\omega)} g_{p+} \tilde{E}_{p+} + i \frac{\Omega_c \tilde{F}_{31} - (\omega + d_{31}) \tilde{F}_{41}}{D_1(\omega)}, \quad (\text{B3c})$$

$$\tilde{S}_{42} = \frac{-\Omega_c}{2D_2(\omega)} g_{p-} \tilde{E}_{p-} + i \frac{\Omega_c \tilde{F}_{32} - (\omega + d_{32}) \tilde{F}_{42}}{D_2(\omega)}, \quad (\text{B3d})$$

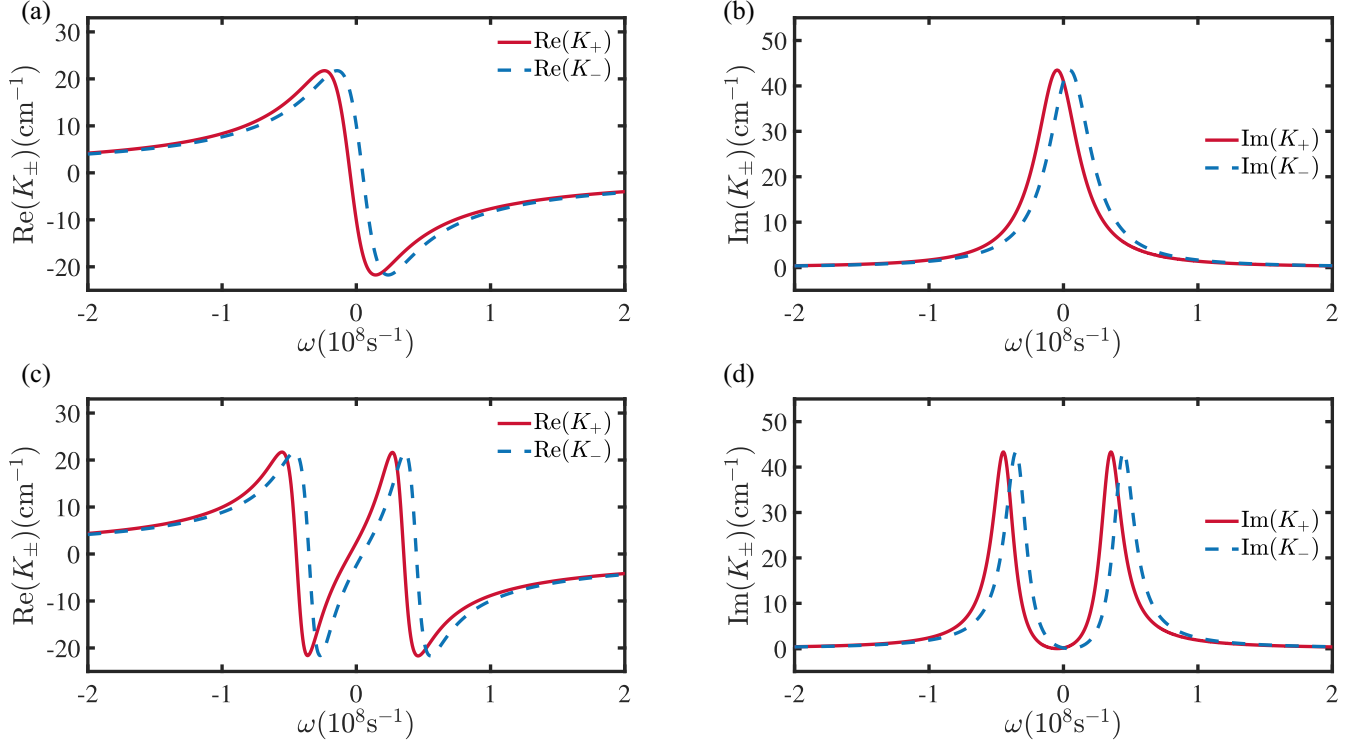


FIG. 9. Linear dispersion relations K_+ (for the σ^+ component) and K_- (for the σ^- component) of the probe field as functions of ω in the absence of the gate atom, with $\Delta_2 = -\Delta_1 = 4.68$ MHz ($B = 1.6$ G), $\Delta_3 = \Delta_4 = 0$, and $\mathcal{N}_a = 3 \times 10^{10}$ cm $^{-3}$. (a) Real parts $\text{Re}(K_{\pm})$ and (b) imaginary parts $\text{Im}(K_{\pm})$ for $\Omega_c = 0$. No EIT occurs in this case. (c) Real parts $\text{Re}(K_{\pm})$ and (d) imaginary parts $\text{Im}(K_{\pm})$ for $\Omega_c = 2\pi \times 6.37$ MHz. An EIT transparency window is opened in both $\text{Im}(K_+)$ and $\text{Im}(K_-)$, i.e., a double EIT occurs.

where $D_{\alpha}(\omega) = |\Omega_c|^2 - (\omega + d_{3\alpha})(\omega + d_{4\alpha} - \Delta_d(z))$ and $Y_{\alpha}(\omega) = \omega + d_{4\alpha} - \Delta_d(z)$ ($\alpha = 1, 2$).

Substituting (B3a) and (B3b) into (B1e) and (B1f), we obtain the two-component envelope equations

$$\left(i \frac{\partial}{\partial z} + K_j(z, \omega)\right) \tilde{E}_{pj}(z, \omega) = i \tilde{\mathcal{F}}_{pj}(z, \omega), \quad (\text{B4})$$

with $j = +, -$. Here

$$K_+(z, \omega) = \frac{\omega}{c} + \frac{|g_p|^2 N}{2c} \frac{[\omega + d_{41} - \Delta_d(z)]}{D_1(\omega)}, \quad (\text{B5a})$$

$$K_-(z, \omega) = \frac{\omega}{c} + \frac{|g_p|^2 N}{2c} \frac{[\omega + d_{42} - \Delta_d(z)]}{D_2(\omega)} \quad (\text{B5b})$$

are the linear dispersion relations of the σ^+ and σ^- components of the probe field, respectively, and the $\tilde{\mathcal{F}}_{pj}(z, \omega)$ are defined by

$$\tilde{\mathcal{F}}_{p+}(z, \omega) = \frac{g_{p+}^* N}{c} \frac{Y_1(\omega) \tilde{F}_{31}(z, \omega) - \Omega_c \tilde{F}_{41}(z, \omega)}{D_1(\omega)}, \quad (\text{B6a})$$

$$\tilde{\mathcal{F}}_{p-}(z, \omega) = \frac{g_{p-}^* N}{c} \frac{Y_2(\omega) \tilde{F}_{32}(z, \omega) - \Omega_c \tilde{F}_{42}(z, \omega)}{D_2(\omega)}. \quad (\text{B6b})$$

Note that in the above derivation, for simplicity, the quantity $\Delta_d(z)$ has been assumed to be a slowly varying function of z , which allows us to take it as a constant during the Fourier transformation.³ The quantity ω in the Fourier transformation (B2) plays the role of the sideband angular frequency of the probe pulse (the center angular frequency is ω_p). Under the

EIT condition, the Langevin noise terms $\tilde{\mathcal{F}}_{pj}(z, \omega)$ are very small and hence can be neglected safely (see detailed discussions of the role of Langevin noise in EIT systems given in Refs. [9,54–56]).

APPENDIX C: DOUBLE RYDBERG EIT FOR $\Delta_d(z) = 0$

If the gate atom is absent, the position-dependent detuning $\Delta_d(z) = 0$. In this case, from (10b) and (10c) we have $K_+(z, \omega) \rightarrow K_+(\omega)$ and $K_-(z, \omega) \rightarrow K_-(\omega)$, with

$$K_+(\omega) = \frac{\omega}{c} + \frac{|g_p|^2 N}{2c} \frac{\omega + d_{41}}{|\Omega_c|^2 - (\omega + d_{31})(\omega + d_{41})}, \quad (\text{C1a})$$

$$K_-(\omega) = \frac{\omega}{c} + \frac{|g_p|^2 N}{2c} \frac{\omega + d_{42}}{|\Omega_c|^2 - (\omega + d_{32})(\omega + d_{42})}. \quad (\text{C1b})$$

Figure 9 shows K_+ (for the σ^+ component) and K_- (for the σ^- component) as functions of ω , plotted by taking $\Delta_2 = -\Delta_1 = 4.68$ MHz ($B = 1.6$ G), $\Delta_3 = \Delta_4 = 0$, and $\mathcal{N}_a = 3 \times 10^{10}$ cm $^{-3}$. From the figure we see that no EIT occurs for either polarization component if the control field is absent, i.e., $\Omega_c = 0$; see the single-peak absorption spectra $\text{Im}(K_+)$ and $\text{Im}(K_-)$ shown in Fig. 9(b). However, when the control field is applied ($\Omega_c = 2\pi \times 6.37$ MHz), an EIT transparency window is opened in both $\text{Im}(K_+)$ and $\text{Im}(K_-)$; see the two-peak absorption spectra plotted in Fig. 9(d). This means that a double EIT occurs in the present inverted-Y system. In particular, when $B = 0$, the two polarization components are nearly degenerate (and hence the level configuration is symmetric) and K_+ and K_- nearly coincide with each other.

APPENDIX D: DERIVATION OF THE RYDBERG-DEFECT POTENTIAL

The preparation of the gate atom results in a position-dependent detuning $\Delta_d(z)$, which induces a Rydberg-defect potential for the propagation of the probe pulse. To show this, we note that Eq. (9) can be written in the form (when neglecting the Langevin noise terms)

$$i\hbar \frac{\partial}{\partial \tau} \tilde{E}_{pj}(z, \omega) = V_j(z, \omega) \tilde{E}_{pj}(z, \omega), \quad (\text{D1})$$

$$\text{Re}[V_+(z)] = \frac{\mathcal{N}_a \omega_p |\mathbf{e}_{p+} \cdot \mathbf{p}_{31}|^2 [\Delta_d(z) + \Delta_1] \{ |\Omega_c|^2 + (\Delta_3 - \Delta_1) [\Delta_d(z) + \Delta_1] + (\Delta_3 - \Delta_1) \gamma_{41}^2 - [\Delta_d(z) + \Delta_1] \gamma_{31} \gamma_{41} \}}{4\epsilon_0 \left[|\Omega_c|^2 - d_{31} [d_{41} - \Delta_d(z)] \right]^2}, \quad (\text{D2a})$$

$$\text{Re}[V_-(z)] = \frac{\mathcal{N}_a \omega_p |\mathbf{e}_{p-} \cdot \mathbf{p}_{32}|^2 [\Delta_d(z) + \Delta_2] \{ |\Omega_c|^2 + (\Delta_3 - \Delta_2) [\Delta_d(z) + \Delta_2] + (\Delta_3 - \Delta_2) \gamma_{42}^2 - [\Delta_d(z) + \Delta_2] \gamma_{32} \gamma_{42} \}}{4\epsilon_0 \left[|\Omega_c|^2 - d_{32} [d_{42} - \Delta_d(z)] \right]^2}, \quad (\text{D2b})$$

$$\text{Im}[V_+(z)] = -\frac{\mathcal{N}_a \omega_p |\mathbf{e}_{p+} \cdot \mathbf{p}_{31}|^2 [\Delta_d(z) + \Delta_1]^2 \gamma_{31} + |\Omega_c|^2 \gamma_{41} + \gamma_{31} \gamma_{41}^2}{4\epsilon_0 \left[|\Omega_c|^2 - d_{31} [d_{41} - \Delta_d(z)] \right]^2}, \quad (\text{D2c})$$

$$\text{Im}[V_-(z)] = -\frac{\mathcal{N}_a \omega_p |\mathbf{e}_{p-} \cdot \mathbf{p}_{32}|^2 [\Delta_d(z) + \Delta_2]^2 \gamma_{32} + |\Omega_c|^2 \gamma_{42} + \gamma_{32} \gamma_{42}^2}{4\epsilon_0 \left[|\Omega_c|^2 - d_{32} [d_{42} - \Delta_d(z)] \right]^2}. \quad (\text{D2d})$$

In deriving the above formula, we have set the two-photon detuning $\Delta_4 = 0$, which is required to obtain a significant EIT effect.

APPENDIX E: INFLUENCE DUE TO THE GATE-ATOM DELOCALIZATION

The calculation results presented in Sec. III were obtained based on the assumption that the gate atom is located exactly at a fixed position $z = z_g = L/2$. This is, strictly speaking, hard to achieve since one cannot determine the exact position of the gate atom due to the intrinsic quantum motion of the atom and also due to other possible noise acting on the atom [17–19]. To be rigorous and also realistic, the influence of gate-atom delocalization should be considered.

To estimate the deviation due to the gate-atom delocalization, we assume that the gate atom may occupy different spatial positions around z_g in a random way. This can be described by the random density distribution of the gate atom with the form $\rho_g(z'_g, \xi) = f(\xi) \delta[z'_g - (z_g + \xi)]$. Here $f(\xi) \equiv (1/\sqrt{\pi}\sigma) \exp[-(\xi/\sigma)^2]$ is a normalized statistical distribution function [$\int_{-\infty}^{\infty} f(\xi) d\xi = 1$], with σ the distribution width and ξ a random variable describing the gate-atom coordinate deviated from the center position $z = z_g$. Hence the position-dependent detuning $\Delta_d(z)$ given in (5) is changed to the form $\Delta_d(z, \xi) = -f(\xi) \frac{C_6}{|(z_g + \xi) - z|^6}$.

Figure 10 shows the result of the numerical simulation on the influence of the gate-atom delocalization to the qubit switch, phase shift, and magnetic-field measurement in the system. Figure 10(a i) illustrates the phase shift ϕ_+ of the σ^+ polarization component of the qubit wave packet as a function of one-photon detuning Δ_3 . The green curve in the figure is the statistical average of ϕ_+ by taking 200 different values

with $\tau \equiv ct$ and $V_j(z, \omega) \equiv -\hbar c K_j(z, \omega)$ ($j = +, -$). One sees that $V_+(z, \omega)$ and $V_-(z, \omega)$ act as external potentials for the σ^+ and σ^- polarization components, respectively. Obviously, the z dependence of $V_{\pm}(z, \omega)$ is a reflection of the Rydberg-defect potential.

Here, for simplicity, we discuss in detail $V_{\pm}(z, \omega)$ near the center point of the EIT transparency windows, i.e., at $\omega = 0$. Based on the result of (10b) and (10c), we have $V_{\pm}(z, 0) \equiv V_{\pm}(z) = -\hbar c K_{\pm}(z, 0) = \text{Re}[V_{\pm}(z)] + i \text{Im}[V_{\pm}(z)]$, with the detailed expressions given by

of ξ , while the red curve is the one for $\xi = 0$, which corresponds to the case where the gate atom is fixed at $z = z_g$. Blue curves in the insets of the figure are the results (describing the fluctuations of ϕ_+) obtained by taking different values of ξ . The system parameters are $L = 80 \mu\text{m}$, $B = 1.4 \text{ G}$, and $\mathcal{N}_a = 3 \times 10^{12} \text{ cm}^{-3}$. Figure 10(a ii) shows the result for the amplitude attenuation factor η_+ (the parameter describing the switch behavior of the system) of the qubit wave packet. In the simulation, 200 different ξ values are chosen between 30 and 50 μm . Since ϕ_- and η_- of the σ^- component behave similarly to those of the σ^+ component, they are not shown here.

Figure 10(b i) illustrates the results of the phase shift ϕ_+ and amplitude attenuation factor η_+ as functions of magnetic field B . Red lines in the figure are for $\xi = 0$ and green lines are for the statistical average by taking 200 random ξ values. The inset of the figure (where blue curves denoting fluctuations are plotted) shows the result obtained by taking different values of ξ . The system parameters chosen here are $\Delta_3 = 0$, $\mathcal{N}_a = 3 \times 10^{12} \text{ cm}^{-3}$, and $L = 100 \mu\text{m}$, with $40 \mu\text{m} \leq \xi \leq 60 \mu\text{m}$. Figure 10(b ii) is similar to Fig. 10(b i) but for the phase shift ϕ_- and the amplitude attenuation factor η_- of the σ^- polarization component.

By inspecting Figs. 10(a i), 10(a ii), 10(b i), and 10(b ii), we see that the green curves (the results of the statistical average for many different random values of gate-atom position) are very closed to the red curves (the results for the fixed position of the gate atom), which means that the influence caused by gate-atom delocalization is small and has no qualitative impact on the main conclusions given in the main text. Thereby, the single-photon qubit switch, phase shifts, and weak-magnetic-field measurement can still be achieved in the system even in the presence of gate-atom delocalization.

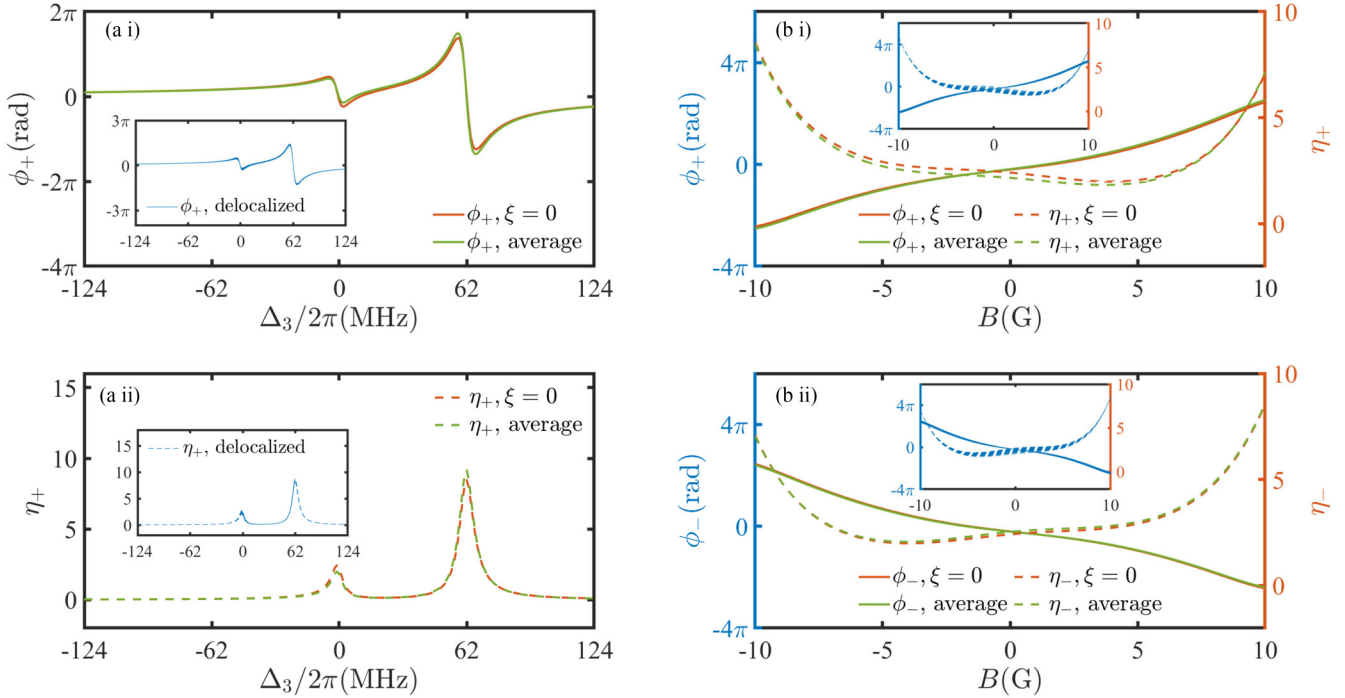


FIG. 10. Influence of the gate-atom delocalization. (a i) Phase shift ϕ_+ of the σ^+ component of the qubit wave packet as a function of one-photon detuning Δ_3 . The green curve is the result of the statistical average by taking 200 different random ξ values (ξ is a random variable describing the coordinate deviation of the gate atom from the center position $z = z_g = L/2$); red line is the result for $\xi = 0$, corresponding to the gate atom fixed at $z = z_g$. Blue curves in the insets are results for different values of ξ . (a ii) Similar to (a i) but for the amplitude attenuation factor of η_+ of the qubit wave packet. (b i) Phase shift ϕ_+ and amplitude attenuation η_+ of the σ^+ component as functions of the magnetic field B . (b ii) Similar to (b i) but for ϕ_- and η_- of the σ^- component. The system parameters are (a i) and (a ii) $L = 80 \mu\text{m}$, $B = 1.4 \text{ G}$, and $\mathcal{N}_a = 3 \times 10^{12} \text{ cm}^{-3}$ and (b i) and (b ii) $\Delta_3 = 0$, $\mathcal{N}_a = 3 \times 10^{12} \text{ cm}^{-3}$, and $L = 100 \mu\text{m}$. One sees that the gate-atom delocalization has no significant influence on the qubit switch, phase shifts, and magnetic-field measurement in the system.

- [1] R. W. Boyd, *Nonlinear Optics*, 3rd ed. (Academic Press, New York, 2008).
- [2] M. Fleischhauer, A. Imamoglu, and J. P. Marangos, Electromagnetically induced transparency: Optics in coherent media, *Rev. Mod. Phys.* **77**, 633 (2005).
- [3] D. E. Chang, V. Vuletić, and M. D. Lukin, Quantum nonlinear optics—photon by photon, *Nat. Phys.* **8**, 685 (2014), and references therein.
- [4] T. F. Gallagher, *Rydberg Atoms* (Cambridge University Press, Cambridge, 2008).
- [5] M. Saffman, T. G. Walker, and K. Mølmer, Quantum information with Rydberg atoms, *Rev. Mod. Phys.* **82**, 2313 (2010), and references therein.
- [6] I. Friedler, D. Petrosyan, M. Fleischhauer, and G. Kurizki, Long-range interactions and entanglement of slow single-photon pulses, *Phys. Rev. A* **72**, 043803 (2005).
- [7] A. K. Mohapatra, T. R. Jackson, and C. S. Adams, Coherent optical detection of highly excited Rydberg states using electromagnetically induced transparency, *Phys. Rev. Lett.* **98**, 113003 (2007).
- [8] J. D. Pritchard, D. Maxwell, A. Gauguet, K. J. Weatherill, M. P. A. Jones, and C. S. Adams, Cooperative atom-light interaction in a blockaded Rydberg ensemble, *Phys. Rev. Lett.* **105**, 193603 (2010).
- [9] A. V. Gorshkov, J. Otterbach, M. Fleischhauer, T. Pohl, and M. D. Lukin, Photon-photon interactions via Rydberg blockade, *Phys. Rev. Lett.* **107**, 133602 (2011).
- [10] O. Firstenberg, T. Peyronel, Q.-Y. Liang, A. V. Gorshkov, M. D. Lukin, and V. Vuletić, Attractive photons in a quantum nonlinear medium, *Nature (London)* **502**, 71 (2013).
- [11] B. He, A. V. Sharypov, J. Sheng, C. Simon, and M. Xiao, Two-photon dynamics in coherent Rydberg atomic ensemble, *Phys. Rev. Lett.* **112**, 133606 (2014).
- [12] P. Bienias, S. Choi, O. Firstenberg, M. F. Maghrebi, M. Gullans, M. D. Lukin, A. V. Gorshkov, and H. P. Büchler, Scattering resonances and bound states for strongly interacting Rydberg polaritons, *Phys. Rev. A* **90**, 053804 (2014).
- [13] T. Caneva, M. T. Manzoni, T. Shi, J. S. Douglas, J. I. Cirac, and D. E. Chang, Quantum dynamics of propagating photons with strong interactions: A generalized input-output formalism, *New J. Phys.* **17**, 113001 (2015).
- [14] M. F. Maghrebi, M. J. Gullans, P. Bienias, S. Choi, I. Martin, O. Firstenberg, M. D. Lukin, H. P. Büchler, and A. V. Gorshkov, Coulomb bound states of strongly interacting photons, *Phys. Rev. Lett.* **115**, 123601 (2015).
- [15] W. Li and I. Lesanovsky, Coherence in a cold-atom photon switch, *Phys. Rev. A* **92**, 043828 (2015).

- [16] M. J. Gullans, J. D. Thompson, Y. Wang, Q.-Y. Liang, V. Vuletić, M. D. Lukin, and A. V. Gorshkov, Effective field theory for Rydberg polaritons, *Phys. Rev. Lett.* **117**, 113601 (2016).
- [17] C. R. Murray, A. V. Gorshkov, and T. Pohl, Many-body decoherence dynamics and optimized operation of a single-photon switch, *New J. Phys.* **18**, 092001 (2016).
- [18] J. D. Thompson, T. L. Nicholson, Q. Liang, S. H. Cantu, A. V. Venkatramani, S. Choi, I. A. Fedorov, D. Viscor, T. Pohl, M. D. Lukin, and V. Vuletić, Symmetry-protected collisions between strongly interacting photons, *Nature (London)* **542**, 206 (2017).
- [19] M. Khazali, C. R. Murray, and T. Pohl, Polariton exchange interactions in multichannel optical network, *Phys. Rev. Lett.* **123**, 113605 (2019).
- [20] K. Jachymski, P. Bienias, and H. P. Büchler, Three-body interaction of Rydberg slow-light polaritons, *Phys. Rev. Lett.* **117**, 053601 (2016).
- [21] S. Das, A. Grankin, I. Iakoupov, E. Brion, J. Borregaard, R. Boddeda, I. Usmani, A. Ourjoumtsev, P. Grangier, and A. S. Sørensen, Photonic controlled-phase gates through Rydberg blockade in optical cavities, *Phys. Rev. A* **93**, 040303(R) (2016).
- [22] L. Yang, B. He, J.-H. Wu, Z. Zhang, and M. Xiao, Interacting photon pulses in a Rydberg medium, *Optica* **3**, 1095 (2016).
- [23] M. J. Gullans, S. Diehl, S. T. Rittenhouse, B. P. Ruzic, J. P. D’Incao, P. Julienne, A. V. Gorshkov, and J. M. Taylor, Efimov states of strongly interacting photons, *Phys. Rev. Lett.* **119**, 233601 (2017).
- [24] M. Moos, R. Unanyan, and M. Fleischhauer, Creation and detection of photonic molecules in Rydberg gases, *Phys. Rev. A* **96**, 023853 (2017).
- [25] Q.-Y. Liang, A. V. Venkatramani, S. H. Cantu, T. L. Nicholson, M. J. Gullans, A. V. Gorshkov, J. D. Thompson, C. Chin, M. D. Lukin, and V. Vuletić, Observation of three-photon bound states in a quantum nonlinear medium, *Science* **359**, 783 (2018).
- [26] S. H. Cantu, A. V. Venkatramani, W. Xu, L. Zhou, B. Jelenković, M. D. Lukin, and V. Vuletić, Repulsive photons in a quantum nonlinear medium, *Nat. Phys.* **16**, 921 (2020).
- [27] P. Bienias, M. J. Gullans, M. Kalinowski, A. N. Craddock, D. P. Ornelas-Huerta, S. L. Rolston, J. V. Porto, and A. V. Gorshkov, Exotic photonic molecules via Lennard-Jones-like potentials, *Phys. Rev. Lett.* **125**, 093601 (2020).
- [28] Y. Ou, Q. Zhang, and G. Huang, Quantum reflection of single photons in a cold Rydberg atomic gas, *Opt. Lett.* **47**, 4395 (2022).
- [29] L. Drori, B. C. Das, T. D. Zohar, G. Winer, E. Poem, A. Poddubny, and O. Firstenberg, Quantum vortices of strongly interacting photons, *Science* **381**, 193 (2023).
- [30] Y. Ding, Z. Bai, G. Huang, and W. Li, Facilitation-induced transparency and single-photon switch with dual-channel Rydberg interactions, *Phys. Rev. Appl.* **19**, 014017 (2023).
- [31] C. Murray and T. Pohl, in *Advances in Atomic, Molecular, and Optical Physics*, edited by E. Arimondo, C. C. Lin, and S. F. Yelin (Academic Press, New York, 2016), Vol. 65, pp. 321–372, and references therein.
- [32] C. S. Adams, J. D. Pritchard, and J. P. Shaffer, Rydberg atom quantum technologies, *J. Phys. B: At. Mol. Opt. Phys.* **53**, 012002 (2020), and references therein.
- [33] Y. O. Dudin and A. Kuzmich, Strongly interacting Rydberg excitations of a cold atomic gas, *Science* **336**, 887 (2012).
- [34] T. Peyronel, O. Firstenberg, Q.-Y. Liang, S. Hofferberth, A. V. Gorshkov, T. Pohl, M. D. Lukin, and V. Vuletić, Quantum nonlinear optics with single photons enabled by strongly interacting atoms, *Nature (London)* **488**, 57 (2012).
- [35] S. Baur, D. Tiarks, G. Rempe, and S. Dürr, Single-photon switch based on Rydberg blockade, *Phys. Rev. Lett.* **112**, 073901 (2014).
- [36] H. Gorniaczyk, C. Tresp, J. Schmidt, H. Fedder, and S. Hofferberth, Single-photon transistor mediated by inter-state Rydberg interactions, *Phys. Rev. Lett.* **113**, 053601 (2014).
- [37] D. Tiarks, S. Baur, K. Schneider, S. Dürr, and G. Rempe, Single-photon transistor using a Förster resonance, *Phys. Rev. Lett.* **113**, 053602 (2014).
- [38] H. Gorniaczyk, C. Tresp, P. Bienias, A. Paris-Mandoki, W. Li, I. Mirgorodskiy, H. P. Büchler, I. Lesanovsky, and S. Hofferberth, Enhancement of Rydberg-mediated single-photon nonlinearities by electrically tuned Förster resonances, *Nat. Commun.* **7**, 12480 (2016).
- [39] D. Tiarks, S. Schmidt, G. Rempe, and S. Dürr, Optical π phase shift created with a single-photon pulse, *Sci. Adv.* **2**, e1600036 (2016).
- [40] F. Ripka, H. Kübler, R. Löw, and T. Pfau, A room-temperature single-photon source based on strongly interacting Rydberg atoms, *Science* **362**, 446 (2018).
- [41] D. Tiarks, S. Schmidt-Eberle, T. Stolz, G. Rempe, and S. Dürr, A photon-photon quantum gate based on Rydberg interactions, *Nat. Phys.* **15**, 124 (2019).
- [42] D. P. Ornelas-Huerta, A. N. Craddock, E. A. Goldschmidt, A. J. Hachtel, Y. Wang, P. Bienias, A. V. Gorshkov, S. L. Rolston, and J. V. Porto, On-demand indistinguishable single photons from an efficient and pure source based on a Rydberg ensemble, *Optica* **7**, 813 (2020).
- [43] J. Vaneecloo, S. Garcia, and A. Ourjoumtsev, Intracavity Rydberg superatom for optical quantum engineering: Coherent control, single-shot detection, and optical π phase shift, *Phys. Rev. X* **12**, 021034 (2022).
- [44] T. Stolz, H. Hegels, M. Winter, B. Röhr, Y.-F. Hsiao, L. Husel, G. Rempe, and S. Dürr, Quantum-logic gate between two optical photons with an average efficiency above 40%, *Phys. Rev. X* **12**, 021035 (2022).
- [45] S. Shi, B. Xu, K. Zhang, G.-S. Ye, D.-S. Xiang, Y. Liu, J. Wang, D. Su, and L. Li, High-fidelity photonic quantum logic gate based on near-optimal Rydberg single-photon source, *Nat. Commun.* **13**, 4454 (2022).
- [46] G.-S. Ye, B. Xu, Y. Chang, S. Shi, T. Shi, and L. Li, A photonic entanglement filter with Rydberg atoms, *Nat. Photon.* **17**, 538 (2023).
- [47] J. Sinclair, D. Angulo, N. Lupu-Gladstein, K. Bonsma-Fisher, and A. M. Steinberg, Observation of a large, resonant, cross-Kerr nonlinearity in a free-space Rydberg medium, *Phys. Rev. Res.* **1**, 033193 (2019).
- [48] Y. Mu, L. Qin, Z. Shi, and G. Huang, Giant Kerr nonlinearities and magneto-optical rotations in a Rydberg-atom gas via double electromagnetically induced transparency, *Phys. Rev. A* **103**, 043709 (2021).
- [49] Z. Shi and G. Huang, Self-organized structures of two-component laser fields and their active control in a cold Rydberg atomic gas, *Phys. Rev. A* **104**, 013511 (2021).

- [50] Z. Shi and G. Huang, Selection and cloning of periodic optical patterns with a cold Rydberg atomic gas, *Opt. Lett.* **46**, 5344 (2021).
- [51] Y. Mu and G. Huang, Stern–Gerlach effect of vector light bullets in a nonlocal Rydberg medium, *Opt. Lett.* **47**, 6221 (2022).
- [52] P. Kok and W. B. Lovett, *Introduction to Optical Quantum Information Processing* (Cambridge University Press, Cambridge, 2010).
- [53] D. Petrosyan and Y. P. Malakyan, Magneto-optical rotation and cross-phase modulation via coherently driven four-level atoms in a tripod configuration, *Phys. Rev. A* **70**, 023822 (2004).
- [54] J. Zhu, Q. Zhang, and G. Huang, Quantum squeezing of slow-light solitons, *Phys. Rev. A* **103**, 063512 (2021).
- [55] J. Zhu and G. Huang, Quantum squeezing of slow-light dark solitons via electromagnetically induced transparency, *Phys. Rev. A* **105**, 033515 (2022).
- [56] J. Zhu, Y. Mu, and G. Huang, Simultaneous quantum squeezing of light polarizations and atomic spins in a cold atomic gas, *Phys. Rev. A* **107**, 033517 (2023).
- [57] D. A. B. Miller, Are optical transistors the logical next step? *Nat. Photon.* **4**, 3 (2010).
- [58] M. A. Nielsen and I. L. Chuang, *Quantum Computation and Quantum Information* (Cambridge University Press, Cambridge, 2000).
- [59] *Optical Magnetometry*, edited D. Budker and D. F. Jackson Kimball (Cambridge University Press, Cambridge, 2013).